Applied Geochemistry 80 (2017) 72–89

Contents lists available at ScienceDirect

Applied Geochemistry

journal homepage: www.elsevier.com/locate/apgeochem

Environmental geochemistry of a mega beach nourishment in the Netherlands: Monitoring freshening and oxidation processes

Iris R. Pit [a, *], Jasper Griffioen [a, b], Martin J. Wassen [a]

[a] Copernicus Institute of Sustainable Development, Utrecht University, The Netherlands
[b] TNO Geological Survey of the Netherlands, The Netherlands

ARTICLE INFO

Article history:
Received 3 October 2016
Received in revised form
2 February 2017
Accepted 3 February 2017
Available online 5 February 2017

Editorial handling by Clemens Reimann.

Keywords:
Cluster analysis
Robust factor analysis
Pyrite oxidation
Coastal management
Sediment
Groundwater

ABSTRACT

As coastal lowlands are prone to sea water flooding, sea-level rise might globally increase this risk. To protect its coastline, the Netherlands adds an average of 12 million m^3 of sand annually, but more is needed to cope with the expected consequences of global warming. In 2011 a novel approach for coastal protection was applied near The Hague, consisting of a mega beach nourishment of 21.5 million m^3 of sand: the Sand Engine – an artificial sand spit rising to 6 m above mean sea level. It uniquely combines coastal engineering construction with environmental, ecological and social considerations. To construct the Sand Engine, material was used from the seafloor, which changed the materials environment from anaerobic to aerobic, triggering two main hydrogeochemical processes: pyrite oxidation and groundwater freshening. The objective of this study was to assess the sediment geochemistry of the Sand Engine and understand the hydrogeochemistry with respect to pyrite oxidation and freshening. When sufficient buffer capacity is lacking, the mobility of metals and metalloids originated from the mineral pyrite, can cause local impacts on ecology and environment. Geochemical and multivariate statistical analyses were performed on 174 sediment samples from the Sand Engine and from material collected from the seafloor prior to its construction, as well as on 86 samples of pore water collected from the Sand Engine. First, a cluster analysis was performed, using model-based (Mclust) and variable clustering. Second, a robust factor analyses (RFA) was used to explain the variation between the groups and discover relationships between elements and/or soil properties within the groups. We distinguished three clusters of sediment samples and two clusters of pore water samples. Sediment cluster 1 was comprised exclusively of surface samples from the Sand Engine; it was differentiated from the other two clusters by its geochemistry, sorting processes and weathering. Sediment clusters 2 consisted of shallow samples from the Sand Engine, as well as deeper autochthone material from the sand pit. Sediment cluster 3 contained deeper samples from the Sand Engine and also shallow autochthone material from the sand pit. Sediment clusters 2 and 3 show differences in carbonate content and, especially, in reactive iron, confirming that in the sand pit area a Holocene marine layer overlies Pleistocene fluvial sand. For the pore water samples, two clusters were estimated: a saline water cluster and a fresh water cluster. Thus the Sand Engine contains source material from two different geological layers, which vary in their reactive iron concentration and carbonate minerals. Pyrite oxidation is seen with depth, resulting in iron oxides and an increase in alkalinity because of calcite dissolution. With the development of the Sand Engine source material is expected to show a decrease in pyrite oxidation, because of low amount of available sulphide minerals. Carbonate dissolution due to pyrite oxidation will then decrease as well. Additional calcite dissolution is caused by freshening processes. With the amount of $CaCO_3$ present in the sand, the Sand Engine contains calcareous-rich sand where acidic conditions are not likely to occur during its life span and therefore create no local environmental risks for acidification. At the surface of the mega beach nourishment, sorting processes are causing locally enrichment of iron oxides and associated elements, as well as a decrease in the stability of heavy minerals like rutile.

* Corresponding author.
E-mail address: i.r.pit@uu.nl (I.R. Pit).

http://dx.doi.org/10.1016/j.apgeochem.2017.02.003

1. Introduction

Coastal management is vital for coastal lowlands in order to protect coastlines from more coastal erosion and flooding due to changing sea levels. In recent decades, coastal defence techniques have gradually changed from primarily hard to primarily soft in both Europe and the USA (Hillyer, 1996; Hamm et al., 2002; Hanson et al., 2002). Hard structures include groynes, seawalls and breakwaters, while soft structures consist of beach restoration and nourishment through sand placement (Hillyer, 1996). Periodic sand nourishment is regarded as an environmentally acceptable method of coastal management and restoration for challenges such as storm-induced erosion, as well as for structural erosion and relative sea-level rise (Hanson et al., 2002).

Global warming is expected to result in sea-level rise (IPCC, 2014; Mengel et al., 2016), so unless a retreating coastline is acceptable, current sea defence strategies need to be adapted (Houghton et al., 2010; Kabat et al., 2009). Together with Spain, the Netherlands has the largest sand nourishment volume in Europe (Hamm et al., 2002). Its nourishment policy, which includes both shoreface and beach nourishment (Rijkswaterstaat, 1990), has been based on an average annual volume of 12 million m^3 of sand at national scale since 2000 (Mulder and Tonnon, 2011; Bakker et al., 2012). Because of sea level rise, it has been proposed to upscale sand nourishments on the Dutch coastline to 85 million m^3 per year (Mulder and Tonnon, 2011). Besides using larger volumes of sand, adapting Dutch coastal management to climate change should also make use of natural processes instead of counteracting them (De Ruig, 1998; Smits et al., 2006). Furthermore, an interdisciplinary approach embedded in a societal context will enhance stakeholders' acceptance of the best options (Nordstrom, 2014). To incorporate these aspects, the innovative 'Building with Nature' paradigm was devised (De Vriend and Van Koningsveld, 2012), and the Sand Engine concept was developed within its context (Mulder and Tonnon, 2011; Stive et al., 2013).

The Sand Engine is a 21.5 million m^3 mega beach nourishment, with an initial surface area of 128 ha applied along the Dutch coast between The Hague and Hoek van Holland in 2011 (Fig. 1 and Fig. 1S). It is the first project in the world that combines coastal engineering construction with environmental, ecological and social considerations (Stive et al., 2013), and in which intensive research is being performed. Initially, the mega beach nourishment spans the coastal system over a 2.4 km stretch and extends up to 1 km offshore consisting of a large hook-shaped peninsula, including a 7.5 ha lake. Due to wind, waves and currents the Sand Engine will gradually change in shape and eventually be fully incorporated into the dunes (Stive et al., 2013). The effectiveness of the mega beach nourishment may lead to exportable technology, which is why its environmental, ecological and social consequences are being evaluated.

Research on beach-related topics is published frequently, but most is related to management, conservation and/or anthropogenic impacts (Nel et al., 2014). Few papers link environmental chemistry and beach ecology with coastal management. Greene (2002) and Nelson (1993) reviewed the biological effects of beach nourishments and the importance of monitoring programmes, which are rarely published in scientific journals (Lindeman et al., 2000). More specifically, McLachlan (1996) observed beach fauna at a specific beach ecosystem and concluded that the alteration of physical conditions affects fauna communities.

To ascertain the environmental impacts of a beach nourishment, it is important to consider the quality of water and soil water (Greene, 2002), but this is not often taken into account. Saye and Pye (2006) examined the geochemistry and particle size of dune sediments along the Danish coast and found that sea sediment applied as beach nourishment causes heavy mineral content to increase, although this could also be because of differences in the composition of the natural source material. Stuyfzand et al. (2012b) compared nourishment material to autochthonous beach and dune material along the Dutch coast and, based on total elemental analysis, showed that nourishment material contains a higher amount of carbonate minerals, Na-silicates and Mg-silicates, and the elements Fe, P, As, Ba, Co, Cs, Ni and Zn. What the available fraction is and how source material and chemical processes influence this fraction was not studied. Therefore, this study examined the impact of a changing environment on the geochemistry of beach nourishment material.

The Sand Engine is made from material dredged from the sea floor. Its construction changed the environmental conditions of the dredged seafloor sediment from anaerobic to aerobic, which triggered biogeochemical processes in the Sand Engine sediment. Two main processes that may alter the geochemistry of the material used to build the Sand Engine and can result in environmental and ecological impacts are pyrite oxidation and freshening. Pyrite (FeS_2) is the most common sulphide mineral in nature. It is stable in anoxic sediments but in the presence of atmospheric oxygen becomes unstable and mobilises its constituents. The interest in pyrite for environmental scientists stems largely from the presence of metals and metalloids that can be incorporated or sorbed to the mineral (Huerta-Diaz and Morse, 1990). However, when sufficient buffer capacity is available, the mobility of metals because of pyrite oxidation is decreased by adsorption to Fe and Mn-oxyhydroxide phases (Cantwell et al., 2008). Oxidation of pyrite can trigger dissolution of calcite, ion exchange and sorption to the iron oxides produced, all of which are key processes in regulating and buffering water quality (Appelo et al., 1998). The instability of pyrite when in contact with atmospheric oxygen makes it likely that pyrite oxidation occurs in the Sand Engine and that its consequences are pronounced in the sediment and water chemistry of the mega beach nourishment.

With a maximum height of 6 m above average sea level, the Sand Engine is freshening because of the infiltration of rainwater. Consequently, cation exchange is expected to occur in the Sand Engine, in which the dominant fresh groundwater ion Ca^{2+} is exchanged for Na^{+} and Mg^{2+} (Appelo and Postma, 2005). Russak and Sivan (2010) found that both K^{+} and Sr^{2+} are also affected by cation exchange enhanced by freshening. The resulting loss of Ca^{2+} from the solution may create undersaturation of calcite, which could lead to calcite dissolution (Sanford and Konikow, 1989).

In addition to pyrite oxidation and freshening, the influence of the construction method on the extent of the geochemical processes also needs to be assessed. To create the Sand Engine, material was transported and deposited via different methods that depended on the local circumstances, project requirements and boundary conditions (Fiselier, 2010). Sand may have been lost during transportation and the fine-grained fraction might have been washed out from the dredger hopper, resulting in an overall larger grain size. Additionally, the different methods used to deposit the sand makes it likely that there are three different degrees of pyrite oxidation at the Sand Engine. The first is minimum oxidation, in sediment that was emptied through the dredger bottom; such sand is now present under water in the deepest part of the nourishment. The second is limited oxidation, in sediment that was sprayed in a high-pressure jet through the air from the dredging vessel (a technique known as rainbowing), and settled below sea level. Finally, there is maximum oxidation, in the surface layer of the rainbowed sediment above sea level.

Our aim was to statistically determine the original geochemistry of the pilot project the Sand Engine and to elucidate the compositional changes of beach nourishment material with respect to

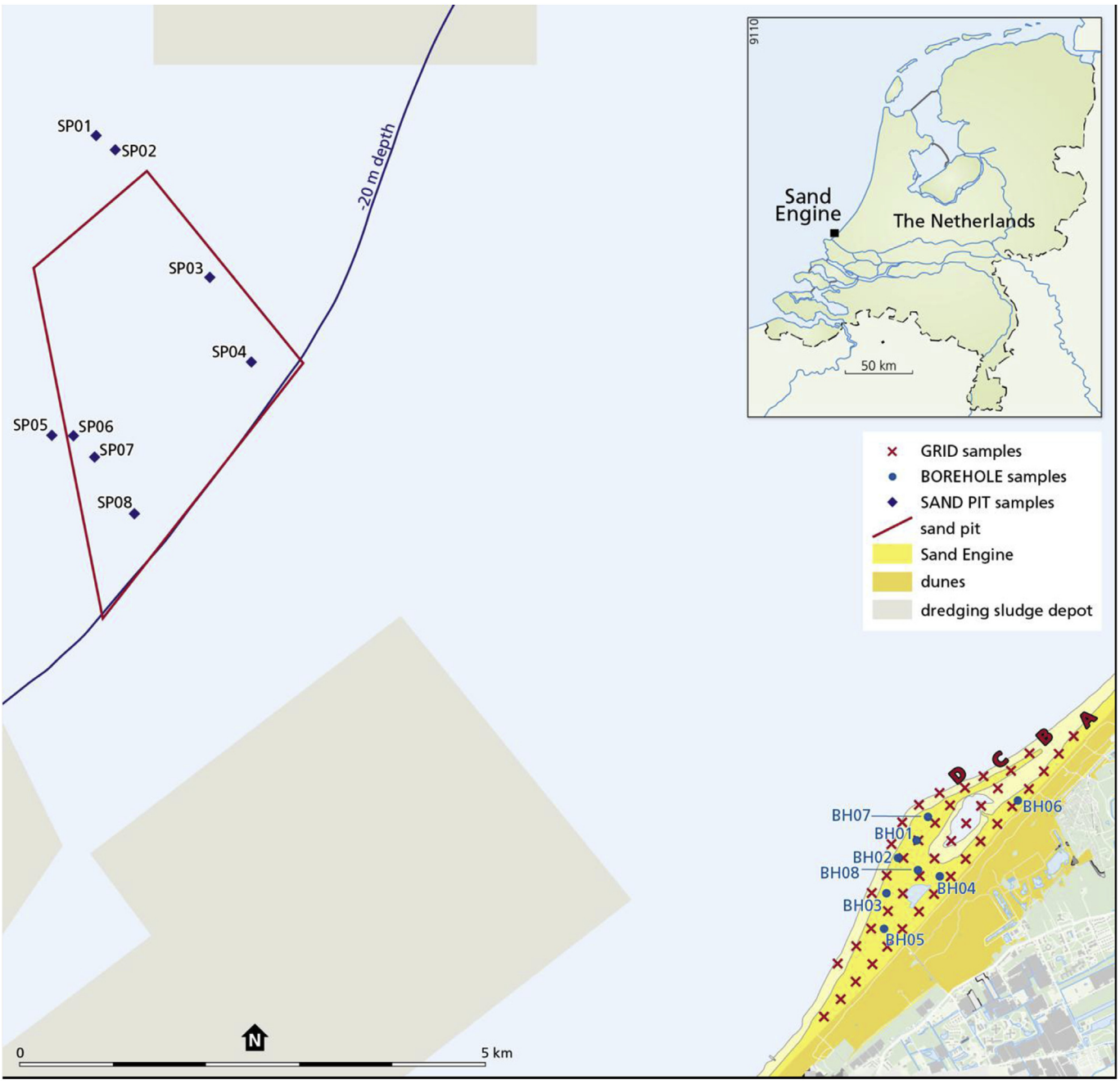

Fig. 1. The location of the Sand Engine, dredging sludge depots and the sand pit, with the sampling locations from GRID, BOREHOLE and SAND PIT.

pyrite oxidation and ion exchange as well as the grain size distribution. We investigated the influence of the construction method and the design of the mega beach nourishment by analysing sediment samples at various depths from the Sand Engine and from the sand pit, which are the submarine pits from which the sand for the Sand Engine was dredged. Finally, we hypothesize if these geochemical processes may have environmental implications.

2. Material and methods

The Sand Engine is a locally concentrated sand nourishment constructed in 2011 from 21.5 million m^3 of sand. This mega beach nourishment is expected to result in a wider beach along a 10–20 km stretch of the Dutch coastline and a beach area gain of 200 ha over a 20-year period (Stive et al., 2013). To construct the Sand Engine, material was dredged from the sea floor 10 km offshore from a sand pit to a maximum depth of 6 m below the sea floor (Fiselier, 2010).

2.1. Sampling

Samples collected from the Sand Engine and the sand pit were assigned to three groups: GRID, BOREHOLE and SAND PIT (Fig. 1). The SAND PIT group comprised 61 sand samples of original material from the areas where the sand pits are now located (SP1 till SP8). The samples had been collected in the period 1970–2001 by

TNO Geological Survey of the Netherlands, for geological research. The sampling techniques used were vibro-core sampling (to a maximum of 4 m depth), grab sampling (to a maximum of 20 cm depth), and flush core sampling (a mixed sample from every 50 cm to a maximum depth of 7 m). The undisturbed cores were stored in an open PVC tube, which was wrapped in thick plastic foil. The grab and flush core samples were put in plastic buckets, which were then closed with a plastic lid. The samples were placed in the core storage facility of TNO, from where we obtained subsamples for this study: we took samples at 50 cm intervals from the undisturbed cores and collected a representative sample with a sand splitter from each grab and flush core.

The GRID group consisted of 46 surface sediment samples and 40 pore water samples from the Sand Engine. Sand was collected laterally in the summer of 2015, using a 250 × 250 m grid with transects A, B, C and D. First, a surface sample of around 500 g was obtained at every point by mixing 5 subsamples from each grid cell: one from the centre and one from the midpoint of each side of a square 2 m across, centred on that point. Second, the bog iron ore fragments ranging in size from 2 to 15 cm long in an area of 4 m^2 around each grid point were counted, because substantial numbers had been observed at the Sand Engine during grid sampling. Eleven bog iron ore fragments were chosen randomly and taken to the lab. Third, pore water was collected from soil samples taken at 50 cm depth, because at this depth the sand contained enough pore water to extract. A 50 cm depth was reached with an Edelman auger and the sand was collected undisturbed in a Ø38 × 240 mm stainless steel core with an Akkerman core sampler. When insufficient soil moisture was found at 50 cm depth, a second stainless steel core was taken just next to the first one. The core was detached from the core sampler and the open spaces were filled with stainless steel fillers and closed with plastic caps. The cores were transported to the lab in a cooler at temperatures comparable to those at the field site where the sediment was centrifuged to separate the pore water from the sediment. The sediment from a core was placed in a plastic centrifuge bottle with a 0.45 μm filter at the bottom and a reservoir below for the pore water that was centrifuged for 30 min at 2000 rpm. A sufficient amount of pore water between 6 and 10 mL was extracted with one or two sediment cores.

For the BOREHOLE group, 67 sand and 46 pore water samples were obtained from eight boreholes (BH01-BH08) in the Sand Engine. The boreholes had been drilled with a sonic drill; two were 20 m deep and six were 10 m deep. The sonic drill contains a 2 m stainless core that brings undisturbed material to the surface. We collected material at various depths straight from the core, using a smaller stainless steel core (Ø38 × 240 mm). The rest of material was placed on an open polyvinylchloride tube for a geological description. At the field site a suitable amount of 10 mL of pore water was immediately extracted from the cores with a rhizon (Seeberg-Elverfeldt et al., 2005). To prevent oxidation of the sand samples, the cores were filled with stainless steel fillers, closed with plastic caps and wrapped in aluminium foil before transportation to the lab at ambient temperatures. The cores were stored in anoxic conditions for three months before further processing.

2.2. Chemical and grain size analyses

We performed chemical analyses on pore water, sand samples and bog iron ore fragments. The pore water was analysed for major and trace elements by using ion chromatography (IC) for Cl, SO_4, NO_2, NO_3, Br and inductively coupled plasma mass spectrometry (ICP-MS) for Na, Mg, Al, P, K, Ca, V, Cr, Mn, Fe, Co, Ni, Cu, Zn, As, Se, Mo, Cd, Sb, Pb. Pore water samples were analysed undiluted except for three samples that contained a small quantity. Alkalinity was measured using a titration method and the pH was determined with a pH meter.

For the sand samples a more elaborate method was chosen. First, the BOREHOLE samples were freeze dried, because of their likely anoxic condition in the field, whereas the GRID and the SAND PIT samples were oven dried at 105 °C for at least 24 h. To obtain the grain size distribution granulometric analyses were performed with a Mastersizer 2000 laser diffraction granulometer (Malvern Instruments Ltd.) after pre-treatment to reduce aggregation of the soil particles, in accordance with NEN 5753 (1990). The SAND PIT samples were not pre-treated because no significant difference was found between the pre-treated and untreated GRID samples. This was probably because of the low contents of organic matter, carbonate cement and clay in the sandy samples.

The second step was to dry sieve the samples in a plastic sieve with nylon cloth to obtain two fractions (<150 μm (>100 mesh) and 150–2000 μm (10–100 mesh)) whose composition could be examined in more detail. According to Pye and Blott (2004), the <150 μm fraction provides a good discrimination between sediment sample types because it contains most of the heavy minerals, micas and clays with which a majority of the trace elements are associated. After sieving, the 150–2000 μm fraction and also the bog iron ore fragments were ground into particles <2 μm with a Herzog HP-PA grinding machine. The total amount of the <150 μm fraction was so small that grinding was not performed, but 10 samples were ground to verify that grinding did not affect chemical analysis.

Both fractions and the bog iron ore fragments were analysed for total C and S contents with the CS elemental analyser. To obtain the thermogravimetric analysis (TGA) for quantitative determination of mineral compounds, the fractions and bog iron ore fragments were heated from 25 to 1000 °C at a heating rate of 1 °C/min using a Leco TGA-601. The aqua regia digestion method described by Houba et al. (1995) was used to obtain the pseudo-total elemental concentrations (Chen and Ma, 2001), which were then analysed with inductively coupled plasma-optical emission spectrometry (ICP-OES) and mass spectrometry (ICP-MS). Finally, 12 samples were analysed using X-ray diffraction (XRD) and scanning electric microscope (tabletop SEM), to obtain qualitative information on their mineralogical and chemical composition.

2.3. Dataset calculations

The statistical data analyses were performed on both the sediment and pore water datasets. For the sediment analyses, stable, non-reactive contents that included the major elements were included. Aluminium is commonly found in feldspars, clays and micas. Since Fe_2O_3, CaO, MgO and MnO occur not only in clays, feldspars and micas but also in oxides, carbonates, sulphides and sulphates, the reactive contents were distinguished from the non-reactive silicate contents, using the correlation with Al_2O_3.

Even though the aqua regia destruction method dissolves mainly reactive contents, non-reactive contents may dissolve as well (Terry, 1983). In order to separate the non-reactive from the reactive contents, the method of Heerdink and Griffioen (2008) was used, with R software (Ihaka and Gentleman, 1996). By performing a quantile regression (QR), a linear baseline is created that separates the non-reactive contents visible close or on the linear baseline from the reactive contents that are seen above the baseline. It is assumed that the reactive contents contain a non-reactive content as well when a clear separation is present. The linear baseline is then used to subtract the reactive content from the total extracted content of each sample and discard the non-reactive content (see Fig. 2). The baseline was estimated with different percentiles that started from 5% and increased by steps of 5%. To determine the accuracy of the different baselines, the Standard Error (SE) was used

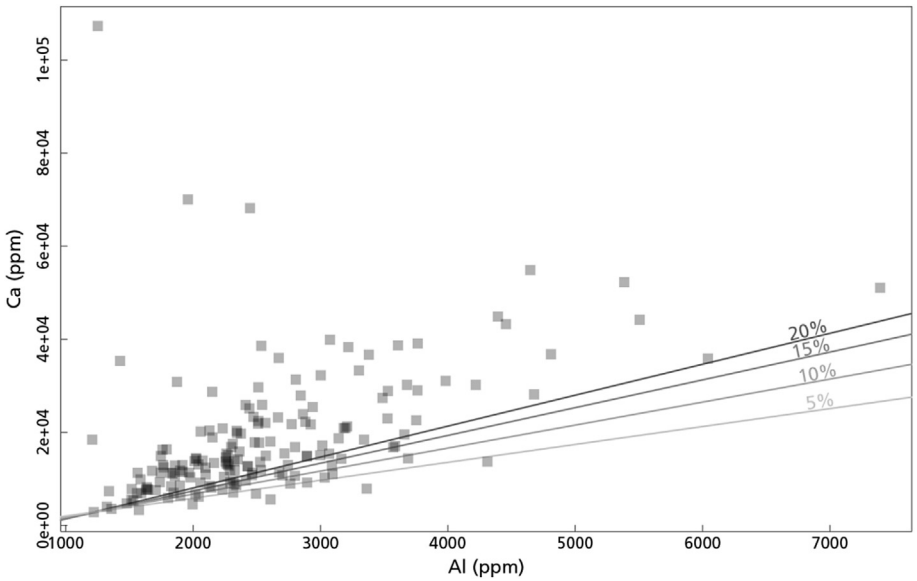

Fig. 2. Baseline estimation of calcium and aluminium, using the Quantile Regression method with steps of 5%.

for the intercept and slope (Moore and McCabe, 1989). The percentile with the smallest band width was considered as the most accurate baseline for calculating the reactive content from the total extracted content. The QR was performed on the elements Fe, K, Mg, Mn, and Na, and separately for the <150 μm and the 150–2000 μm fractions because of the mineralogical variability between grain size classes. No division was made among the groups, because all the sand came from a similar source.

The raw data from the TGA was smoothed by using the Gaussian smoothing algorithm (Liu et al., 2004) with the PeakFitTM software (SPSS Inc.) to exclude the noise from the thermographs. Using the smoothed TGA data, the first derivative (DTG) with respect to either time or temperature was obtained by calculating the difference in weight loss per minute, which improves the resolution and presents the specific temperature characteristics more accurately (Földvári, 2011). The organic material was estimated from the DTG from the weight loss between 105 and 550 °C and the concentration of carbonate minerals between 550 and 850 °C. Visible peaks contained values consistently above 0.002%. Lower values were considered negligible and therefore excluded from the total weight loss.

The Ca concentration derived with the aqua regia method was assumed to be reactive carbonate as described in section 3.1.3 and therefore the $CaCO_3$ content obtained from the TGA was not included in the statistical analyses.

2.4. Multivariate statistical data analysis

The complete geochemical dataset was used to test whether the geochemistry of the Sand Engine is influenced by hydrogeochemical processes as well as by the grain size distribution. First, a cluster analysis (CA) was performed on both the pore water and sediment dataset, as an exploratory data analysis. The CA for the pore water dataset was used to investigate oxidation and freshening processes, whereas the CA for the sediment dataset was to evaluate the characteristics and compositional overlap between the three groups GRID, BOREHOLE and SAND PIT, and to extract more homogeneous data subsets, which were subsequently used for robust factor analysis (RFA).

The CA consisted of both model-based clustering (Mclust) and variable clustering. The Mclust provides the most reliable and best interpretable results when a dataset consists of a high number of observations and variables (Templ et al., 2008; Reimann et al., 2008). The Expectation Maximisation algorithm used selects the cluster models (e.g. spherical or elliptical cluster shape) and determines the cluster memberships of all samples for solutions over a range of different numbers of clusters.

The RFA was used to explain the variation between the groups and discover relationships between elements and/or soil properties within the different groups (Filzmoser et al., 2009). It defines the variation in a multivariate data set by as few controlling factors as possible and detects hidden multivariate data structures (Reimann et al., 2008). The results of the RFA contain factor loadings and factor scores. The factor loadings indicate how each hidden factor is associated with the variables used in the analysis and is scaled from +1 via 0 to −1. The factor scores indicate how strongly each sample is connected to the factor loadings, by showing positive and negative values per sample.

Prior to the statistical analysis, the data set was prepared by changing censored data values and removing data outliers. Censored data values are values below a detection limit: they were set at a value half the detection limit (Reimann et al., 2008). When more than 25% of the values of a variable were below the detection limit, the variable was excluded from the multivariate statistical analysis.

Data outliers are common in geochemical datasets and are not extreme values of a normal distribution but values originating from various processes, such as contamination. Outliers can strongly influence CA, because of the disturbance of homogeneous clusters; the simple option would be to delete the outliers beforehand (Templ et al., 2008). According to Reimann et al. (2008), the most reliable method of detecting data outliers is to combine the MEDIAN ± 2 · MAD (Mean Absolute Deviation) rule and a boxplot.

The outliers found for the sediment dataset were in 11 samples of the 150–2000 μm fraction and 14 samples of the 0–150 μm fraction. In total 5 samples were removed prior to CA and RFA because they contained more than 3 variables as outlier. We removed 3 samples from the 0–150 μm fraction (all from the GRID group), which are situated in the intertidal area at different locations at the Sand Engine. Two samples from the 150–2000 μm

fraction (both from the SAND PIT group) were removed, because of outliers for Al, Fe and many REE elements that may be caused by local secondary enrichments as coatings. Four samples of the pore water dataset were identified as outliers: as they were distributed among the variables Al, Co, Sb and Zn, no samples were excluded from the CA. Not all pore water variables were taken into account, because 25% or more of the values of Br, Cd, Cr, NO_2, NO_3, Pb and Se were below detection limit.

The data was log-ratio transformed in order to "open" closed data. Geochemical datasets often contain individual variables that are related to each other which is being expressed as a percentage or parts per million, and which sum to a constant like 100% or 1. Those are referred to as compositional data or closed data (Aitchison, 1982). Variables expressed as percentage data do not vary independently; to remove the effects of closure, data needs to be transformed. The simple log transformation was used for the outlier detection and the CA. For the RFA the isometric log-ratio (ilr) transformation was used, which was introduced by Egozcue et al. (2003) and often proves to be the preferred log-ratio transformation for environmental data (Filzmoser et al., 2009). With ilr-transformed data, a robust estimation of the covariance matrix is obtained, which is then back-transformed to centred log-ratio (clr) space for maintaining the links to the original variables and enabling direct interpretation. For both the CA and the RFA the data was standardised (scaled and centred) to make trace elements comparable to major elements. The sediment variables used for the CA and RFA were Al, As, Ba, Ca, Cd, Cr, Cu, reactive Fe (Fe_r), K, Mg, Mn, Mo, Na, Nb, Ni, P, Pb, Sb, Sc, Se, Sr, Ti, V, Zn, Zr, C, S. The organic material fraction was not taken into account for statistical analysis because several samples from the GRID group as well as a few from the BOREHOLE group contained a negligible amount of organic matter, because it was below detection limit.

2.5. Freshening

The chemical reactions occurring during fresh water displacement can be elucidated by comparing the measured water composition with the composition for conservative mixing of fresh water and sea water. The fraction of sea water (f_{sea}) is calculated from the Cl concentration (Appelo and Postma, 2005):

$$f_{sea} = \frac{m_{Cl,sample} - m_{Cl,fresh}}{m_{Cl,sea} - m_{Cl,fresh}} \quad (1)$$

The conservative mixing concentration ($m_{i,mix}$) for other dissolved species is calculated from:

$$m_{i,mix} = f_{sea} \cdot m_{i,sea} + (1 - f_{sea}) \cdot m_{i,fresh} \quad (2)$$

where $m_{i,sea}$ and $m_{i,fresh}$ are the concentrations in sea water and fresh water of the species i, respectively. The concentration for fresh water was derived from Stolk (2001) and for sea water from Appelo (1994). The enrichment or depletion (Δm_i) of the species i is then obtained by:

$$\Delta m_i = m_{i,sample} - m_{i,mix} \quad (3)$$

A positive Δm_i indicates pore water to be enriched for species i and a negative Δm_i indicates depletion compared to solely mixing.

Freshening as well as a decrease in pH may cause calcite dissolution (Appelo and Postma, 2005). To ascertain whether the saturation state for calcite is decreasing in the Sand Engine, the saturation index (SI = log(IAP/K) where IAP is the ion activity product) for calcite was calculated using the geochemical code PHREEQC (Parkhurst and Appelo, 2013). The sandy unsaturated zone is probably an open system with rapid gas exchange through the gas phase (Laursen, 1991), and with infiltrating rain water the calcite dissolution is expected to be fast in the unsaturated zone of the Sand Engine (Wijnakker, 2015). The expected HCO_3^- concentration was calculated to estimate calcite dissolution in an open unsaturated system and compared with the measured HCO_3^- concentration, in order to assess the impact of additional calcite dissolution processes like freshening and pyrite oxidation. Calcite dissolution in an open system depends on the amount of CO_2 dissolved in water. Partial pressures of CO_2 (P_{CO_2}) were calculated from alkalinity and pH analyses using PHREEQC. The related equations are:

$$\log\left[H_2CO_3^*\right] = 6.3 + \log\left[HCO_3^-\right] + \mathrm{pH} \quad (4)$$

$$\log\left[P_{CO_2}\right] = \log\left[H_2CO_3^*\right] + 1.5 \quad (5)$$

For a given P_{CO_2} the concentration of HCO_3^- was calculated via the following equation (Appelo and Postma, 2005):

$$m_{HCO_3^-} = 2 \cdot \sqrt[3]{10^{-6}\left[P_{CO_2}\right]/4} \quad (6)$$

3. Results & discussion

Below, we first describe the general characteristics of the samples. Then, the sediment dataset with the results of the QR, the CA and the RFA is presented, and the source material, carbonate minerals and bog iron ore fragments are discussed. Finally, the CA and RFA results for the pore water dataset are given and the pyrite oxidation and freshening are discussed. Depth indications of the boreholes are with respect to ground level unless mentioned otherwise.

The general characteristics were calculated from the results of the two fractions, 0–150 μm and 150–2000 μm, based on the percentage for the grain size distribution (Table 1). From the grain size distribution it is clear that overall the samples contain sand with a median grain size of around 350 μm. The GRID samples are coarsest, with the lowest range in $CaCO_3$ and organic material. Stuyfzand et al. (2012b) found similar results for samples collected at the Sand Engine during construction in 2011, with mean grain size distribution of 318–515 μm. The $CaCO_3$ found is somewhat higher compared to this study with means ranging from 1.7 till 9.0% and is more comparable to the BOREHOLE samples. This suggests that the grain size distribution at the surface of the Sand Engine has been affected by sorting processes like aeolian activity and probably also by dredging activities and that $CaCO_3$ mineral contents are decreased by chemical processes after construction of the Sand Engine. Sorting processes through aeolian activity are seen clearly for the GRID samples where finer material is present towards the dune area with a median of 2.5% <150 μm, which is higher than the median of 0.1% of <150 μm close to the waterline.

A total of 16 sediment samples, 8 from the BOREHOLE group and 8 from the SAND PIT group, contained clay (defined as grain size smaller than 2 μm) in a range of 0.24–1.56%. Silt and clay layers were also found in the geological descriptions of the boreholes: one silt layer in BH03 at a depth of 8.6 m, one thin clay layer of 20 cm present in BH07 at a depth of 12.8 m and three in BH08 at depths below 10.5 m. Unfortunately, these silt and clay layers were too thin to sample separately without interference from other material. Nourishment material was present to a depth of around 12.8 m in BH07, to a depth of around 9.7 m in BH08 and to a depth of about 8 m in BH03, which means the silt layer and clay layers lie below the nourishment material and may contain original material or

Table 1
Median, 25-percentile and 75-percentile results (in % of dry weight) of $CaCO_3$ and organic matter. Also grain size distribution for each sample group (GRID, BOREHOLE and SANDPIT) is given.

	n	$CaCO_3$			Organic matter			D50	<150 μm
		median	25-percentile	75-percentile	median	25-percentile	75-percentile	median	median %
GRID	46	2.87	2.09	4.76	0.10	0.01	0.54	367	0.95
BOREHOLE	67	4.71	3.42	8.11	0.90	0.08	1.01	341	3.24
SAND PIT	61	4.14	2.95	5.98	0.76	0.67	0.85	329	2.76

older nourishment material. BH05 is a relatively coarse core: several layers contain abundant shell fragments.

3.1. Sediment

It was attempted to separate the non-reactive contents of the sediment dataset from the reactive contents by using the QR method (Fig. 2). The Al content of all samples was below 4%, which means feldspars predominate over clay minerals (Schokker et al., 2005; Huisman and Kiden, 1998; Dellwig et al., 1999), and a distinction between high and low Al content was not necessary. According to Boggs (2009) feldspars, muscovite and biotite commonly occur in the silt and sand fraction. The low amount of silt and clay minerals in the samples was confirmed by the grain size distribution: the median of <63 μm was 0% for both the GRID and BOREHOLE group and 0.01% for the SAND PIT group. For the aqua regia analyses, only Fe was found to have significant reactive and non-reactive contents: the 35 percentile baseline was most accurate for the 0–150 μm fraction whereas the 15 percentile baseline was most accurate for the 150–2000 μm fraction. It is commonly assumed that the baseline for Dutch sediments is the 25 percentile (Huisman, 1998; Griffioen et al., 2016). The baselines we found may be the result of dividing the samples into two fractions and of aqua regia analysis instead of XRF analysis that yields total elemental contents.

3.1.1. Cluster analysis

The statistical analysis started with the CA and resulted in 3 clusters for the fine (F) 0–150 μm fraction as well as for the coarse (C) 150–2000 μm fraction (Table 2). Each cluster is differentiated from the other clusters by means for each variable, which is a value for cluster centre: high or low means for an element suggest high influence of this element on the observations in the corresponding cluster (Table 1S).

For the 0–150 μm fraction (fine) the first cluster contains only samples from the GRID group, in which high positive means are seen for heavy mineral related elements such as Se, Zr and Ti. The negative means were most significant for Nb, S and Na. Cluster 2_F contains samples from both the BOREHOLE and SAND PIT groups; with one exception (a sample from 12 m depth), the samples from the BOREHOLE group were down to a depth of 9.5 m, whereas the samples from the SAND PIT group were all from deeper than 1.5 m below the sea floor and most were from 4 to 7 m depth. For this cluster, the means were positive for the carbonate variables and negative for heavy metals like As and Zr. Cluster 3_F contained samples from all groups: the GRID samples came from close to or at the waterline, whereas the BOREHOLE samples were from various depths and, with one exception (a sample from 6 to 7 m below the sea floor), the SAND PIT samples were shallow (from the sea floor to a depth of 3 m below the sea floor). The highest positive means for Cluster 3_F are for S and Na, but overall the means are negative, with carbonate variables most significant, including the means for Ca, C, Sr, Mg and Mn.

For the 150–2000 μm fraction (coarse), Cluster 1_C contains only surface samples originating from the GRID group and differs from the other clusters by having a greater abundance of heavy mineral related elements, including Zr, Sc and Ti. Clusters 2_C and 3_C contain samples from both the BOREHOLE and the SAND PIT groups: Cluster 2_C has mainly shallow samples from the BOREHOLE group (maximum depth of 9.5 m), plus one sample from 12.7 m below surface. The SAND PIT group comprised deeper samples, with most from 4 to 7 m below the sea floor. The important variables in this cluster show mainly negative means, with the most significant being reactive Fe, together with Zn and P. The opposite is visible for Cluster 3_C compared to Cluster 2_C: only samples below average sea level are included from the BOREHOLE group. From the SAND PIT group, the shallow samples are included to a maximum of 4 m below the sea floor, except for two samples that are deeper. Cluster 3_C shows a balance of both negative and positive means, with heavy mineral related elements including Zr, Ti and Sc having negative means and Nb, Na, Mo and Mn having positive means.

Both the coarse fraction and the fine fraction show a combination of shallow samples from the boreholes and deep samples from the sand pit in one cluster (Table 2). This is logical, given the dredging history. In the Netherlands, sand is usually dredged by a trailer suction hopper: the vessel removes material from the sea floor using one or two suction pipes, leaving grooves 1–2 m wide and 20–50 cm deep (Phua et al., 2002). Therefore, sand from the shallow part of the sand pit is likely to have filled the deepest part of the nourishment and sand from the deeper part of the sand pit will probably be abundant in the shallow part of the nourishment. Based on the samples included in each cluster, we derived the following characterisation: Clusters 1_F and 1_C are surface clusters, Clusters 2_F and 2_C are shallow Sand Engine clusters (= deep sand pit clusters), and Clusters 3_F and 3_C are deep Sand Engine clusters (= shallow sand pit clusters). Nourishment material is estimated to be present down to around 10 m below the surface of the Sand Engine. Material below the nourishment was sampled as well and assigned to the BOREHOLE group. These samples are

Table 2
The distribution of the samples of each cluster estimated by Mclust compared to the sample groups GRID, BOREHOLE and SAND PIT.

	Fine fraction				Coarse fraction			
	n	Cluster 1_F	Cluster 2_F	Cluster 3_F	n	Cluster 1_C	Cluster 2_C	Cluster 3_C
GRID	43	37	0	6	46	46	0	0
BOREHOLE	67	0	30	37	67	0	28	39
SAND PIT	61	0	32	29	59	0	16	43

included in Clusters 3_C and 3_F, which indicates the material is related to the shallow samples from the SAND PIT group.

To differentiate by source material it is preferable to take the coarse grain size fraction, as <200 μm grains are transported more easily by wind and in suspension, which can lessen differences in the mineralogical composition of the geological layers (Eisma, 1968).

3.1.2. Robust factor analysis

The results of the RFA presented in Table 3 allow for interpretation of the related variance within each cluster: negative significant loadings give an estimation of a possible inverse relationship with the positive significant loadings. Overall, the coarse fraction shows a clear pattern, whereas the pattern for the fine fraction is less distinct. All clusters, except for Cluster 2_F, show a significant contribution of carbonate minerals in the first factor that explains at least 41% of the variance. Besides that, reactive Fe and associated variables, including V and As, are important in each cluster, as well as silicate-related elements such as Al, Ba, K and Na. Although the presence of silicate minerals is apparent, a clear pattern may not always be present within the clusters, as many silicate minerals do not completely dissolve with the aqua regia destruction (Chen and Ma, 2001). Sea water contributed to the Na concentration in sand samples and is estimated with a correction factor described by Stuyfzand et al. (2012a). The contribution is seen for Cluster 1_C and Cluster 1_F and only for the second factor, where samples from the intertidal area show a sea water contribution between 341 and 2580 ppm. The sea water contribution depends on the soil moisture content and porosity of the sand, which varies between surface samples and depth samples. Sulphur is present in the significant negative loadings in the fourth explanatory factor of the fine fraction (Clusters 1_F and 3_F), indicating that sulphur minerals are

Table 3
Results of the robust factor analysis for three clusters of the fine fraction (F) and the coarse fraction (C), with the interpretation of the first four factors representing the variables with a significant positive loading (r larger than 0.7 and 0.5) as well as the variables with a significant negative loading (r lower than −0.7 and −0.5).

	Factor	% of explained variance		Significant positive loadings		Significant negative loadings	Interpretation minerals
Cluster 1_F	1	42%	r > 0.7	Ca, Sr, C, Mg, Al, Ba	r < −0.7		Positive: carbonate minerals, silicate minerals
			r > 0.5	Zn	r < −0.5	Na, Nb	Negative: silicate minerals (Na-feldspars)
	2	14%	r > 0.7	Fe_r, V, Ti, As, Pb, Se	r < −0.7	Na	Positive: Fe-minerals (oxides), heavy minerals
			r > 0.5	Nb, P, Cr	r < −0.5		Negative: Na-feldspars, sea water contribution
	3	11%	r > 0.7	Sc	r < −0.7		Positive: silicate minerals
			r > 0.5	Ni, Zn	r < −0.5	Cu	Negative: –
	4	4%	r > 0.7		r < −0.7	S	Positive: heavy minerals
			r > 0.5	Sb, Zr, Cu	r < −0.5	K	Negative: silicate minerals, S minerals
Cluster 2_F	1	69%	r > 0.7	K, Zr, S, Cd, Ba	r < −0.7		Positive: silicate minerals
			r > 0.5	Al, As	r < −0.5	Fe_r, Cr	Negative: Fe minerals
	2	6%	r > 0.7	Sr, Ca, C, Mn	r < −0.7		Positive: carbonate minerals and Mn-oxides
			r > 0.5	Sc	r < −0.5		
	3	4%	r > 0.7	Zn, Ni, Al, Mg	r < −0.7		Positive: silicate minerals
			r > 0.5	Cu	r < −0.5		
	4	3%	r > 0.7	Ti, V	r < −0.7		Positive: heavy minerals
			r > 0.5		r < −0.5	Na	Negative: Na-feldspars
Cluster 3_F	1	43%	r > 0.7	Ca, Mg, Sr, C	r < −0.7		Positive: carbonate minerals
			r > 0.5	Ni	r < −0.5		
	2	13%	r > 0.7	Zr, Al, K, Ba	r < −0.7	Fe_r	Positive: silicate minerals (mica, feldspars, heavy minerals)
			r > 0.5	Sc	r < −0.5		Negative: Fe minerals
	3	11%	r > 0.7	Ti, Nb, Se,	r < −0.7		Positive: silicate minerals
			r > 0.5	Sc, Cr, P	r < −0.5		
	4	4%	r > 0.7		r < −0.7		Positive: oxides
			r > 0.5	Sb, Zn, Cd, Pb	r < −0.5	S, As	Negative: S minerals
Cluster 1_C	1	47%	r > 0.7	Ca, Sr, Ti, C, Mn	r < −0.7		Positive: carbonate minerals, Mn oxides
			r > 0.5	Mg, Cr	r < −0.5	Ba, Pb	Negative: silicate minerals
	2	11%	r > 0.7	As, V, Fe_r, Zn, Sb	r < −0.7		Positive: Fe minerals
			r > 0.5		r < −0.5	Na, Mg	Negative: silicate minerals, sea water contribution
	3	10%	r > 0.7	Al	r < −0.7		Positive: Al minerals
			r > 0.5	K, Ba, Ni, Sc	r < −0.5	P	Negative: Ca–Fe-phosphates
	4	6%	r > 0.7		r < −0.7		Positive: –
			r > 0.5	Cu, Se	r < −0.5	Na	Negative: Na-feldspars
Cluster 2_C	1	50%	r > 0.7	Ca, C, Sr	r < −0.7	Fe_r	Positive: carbonate minerals
			r > 0.5	Mn, Mg	r < −0.5	V, As	Negative: Fe minerals
	2	14%	r > 0.7	Sc, Ti, Mg	r < −0.7	Cd, Mo	Positive: silicate minerals (feldspars)
			r > 0.5	Al, Ni, Mn, Na	r < −0.5	P, As, V	Negative: (Fe) oxides
	3	6%	r > 0.7	Ba, Zr	r < −0.7		Positive: silicate minerals
			r > 0.5	K, Se	r < −0.5		
	4	4%	r > 0.7	Sb	r < −0.7		Positive: oxides
			r > 0.5	Nb	r < −0.5		
Cluster 3_C	1	41%	r > 0.7	Sr, C, Ca	r < −0.7	Fe_r, As, Sb, Pb, P	Positive: carbonate minerals (calcite), Al minerals
			r > 0.5	Mg, Cu, Al, K, Cr	r < −0.5	V, Zn	Negative: Fe minerals
	2	18%	r > 0.7	Ti, Mn, Sc	r < −0.7		Positive: silicate minerals
			r > 0.5	Cr, Mg, Ni, Al	r < −0.5	Mo, Cd	Negative: –
	3	11%	r > 0.7	Ba	r < −0.7		Positive: silicate minerals (mica, feldspars)
			r > 0.5	Ni, Se, Cu, K	r < −0.5	Zn, V, P	Negative: Fe (oxides)
	4	7%	r > 0.7		r < −0.7		Positive: silicate minerals
			r > 0.5	Nb, Na, Sc	r < −0.5	Se	Negative: –

present in the Sand Engine, but the significance is low. See section 3.2.1 for a more detailed description on the presence of pyrite in the Sand Engine. Also, Ti is seen to be important in the clusters, but is connected to different variables; below, the most important factors are described that explain a variance of >10%. The interpretation of the other explanatory factors is presented in Table 3.

For the surface Cluster 1_C, the first factor (47% variance explained) shows significant positive loadings of Ti, Cr and carbonate variables including C, Sr, Ca, Mg and Mn, where Ti implies the presence of heavy minerals like rutile (TiO_2), ilmenite ($FeTiO_3$) or titanite ($CaTiSiO_5$). The significant negative loadings are Ba and Pb, and these correlate well with Al (>0.60), K (>0.64) and Zr (>0.65), which indicate silicate minerals. The distribution of the scores is highly positive for samples from the high part of the Sand Engine and negative for samples from the intertidal area of the Sand Engine, which suggests that both sea water and sorting processes may have influenced the geochemistry. Silicate minerals are more evenly divided over the two fractions whereas carbonate minerals are significantly higher in the fine fraction, with a median of 18.7± 6.3% $CaCO_3$ compared to 3.6± 3.3% $CaCO_3$ for the coarse fraction. The grain size distribution is coarser close to the waterline, which may indicate that sorting processes have an influence on the first explanatory factor. The second factor, which explains 11% variance, includes the variables As, V, reactive Fe, Zn and Sb. Each of these variables correlates strongly with reactive Fe (>0.85) and with the presence of reactive Fe, iron oxyhydroxides are most likely where Fe acts as a sink because of the high sorption capacity for trace elements (Acosta et al., 2011). Positive scores are seen close to the dune area and indicate that sorting processes may have an influence at the surface of the Sand Engine, as Fe_r shows a higher concentration in the finer fraction (median of 1.14± 0.37% Fe_r compared to 0.33± 0.1% Fe_r for the coarse fraction). Negative significant loadings are Na and Mg: their correlation with Al is similar to that for the first explanatory factor. The correlation between Na and Al shows the presence of Na-feldspars; when random samples were studied, albite was found with the XRD.

Cluster 2_C shows for the first factor 50% variance explained by the carbonate mineral elements Ca, C, Sr, Mn and Mg. The scores indicate a source-related relationship: scores are positive for the BOREHOLE group at various depths and for the SAND PIT group at 3–7 m depth. Negative significant loadings contain reactive Fe and trace elements, which seems to indicate Fe minerals like oxyhydroxides for the first factor as well as for the third factor that explains 14% of variance. Given that there are negative scores for samples from the BOREHOLE group and no samples from the SAND PIT group, this may show the presence of oxidation processes. For the second factor (14% of the variance explained), many variables are significantly positively loaded. A link can be made to silicate minerals and potentially augite $(Ca,Mg,Fe)_2(Si, Al)_2O_6$, which is considered to be an important heavy mineral for fluvial Rhine deposits in the North Sea (Schüttenhelm and Laban, 2005). The positive scores are similar to those for the first explanatory factor and may also show a source-related relationship. Significant negative loadings contain the trace elements Cd, Mo, P, As and V, and here, too, a source-related relationship is likely, because the negative scores are seen for samples from the BOREHOLE group at various depths as well as for some samples from the SAND PIT group.

Cluster 3_C shows for the first factor 41% variance explained by variables of carbonate minerals and silicate minerals. Similar to Cluster 2_C, the positive scores indicate a source-related relationship, with positive scores for BOREHOLE samples from depths below sea level as well as for SAND PIT samples from depths below 1.5 m. For the negative loadings, Fe mineral variables are significant with Fe_r, As, Sb, Pb, P, V and Zn, and negative scores only for samples from the SAND PIT group from 0 to 2 m depth. The second factor (18% of the variation explained) shows significant positive loadings for silicate-related elements with Ti, Sc, Ni, Cr and Al, and also with Mg and Mn. The scores are positive only for SAND PIT samples from depths between 1.5 and 7 m. For the negative loadings, Mo and Cd are significant and there are negative scores for the deeper samples from the BOREHOLE group.

The first cluster of the fine fraction, Cluster 1_F, deserves to be explained in more detail because of its differences and its overlap with Cluster 1_C. For the other clusters, only the first explanatory factor is described. The first factor of Cluster 1_F shows that variables of silicate minerals as well as carbonate minerals explain 42% of the variance: Ca, Sr, C, Mg, Al, Ba and Zn. Positive scores are for samples from the higher, fresh parts of the Sand Engine, mainly in the northern part towards the dune area, which may indicate enrichment through sorting processes. There are significant negative loadings for Na and Nb, which suggests the presence of Na-feldspars; negative scores are seen close to the waterline. The second factor shows significant positive loadings for reactive Fe and highly correlating elements Ti, As, Pb and Se: this may indicate Fe minerals like iron oxides and/or ilmenite ($FeTiO_3$). The scores are positive at the same locations as for the first factor, which suggests sorting processes may play a role in this factor too. The significant negative loading is for Na, which correlates only positively with Cu and Zr and might be related to heavy minerals. The negative scores are also similar to the first factor, which may therefore indicate sorting processes as well, where heavy minerals are more likely to be preferentially present in a dynamic intertidal area than lighter minerals.

For the first factor (69% of the variance explained), Cluster 2_F shows many significant positive loadings (K, Zr, S, Cd, Ba, Al, As) and indicates silicate and S minerals. The scores are positive for the BOREHOLE samples (from depths between 5.8 and 9.4 m). Scores are negative for SAND PIT samples, with negative significant loadings of reactive Fe and Cr: possible minerals are Fe-oxides and chromite ($FeCr_2O_4$). Cluster 3_F shows a first factor with 43% of variance explained: there are positive significant loadings for carbonate mineral elements, with Ni being most correlated with Mg (0.79). The negative significant loadings are for reactive Fe and neither the positive scores nor the negative scores show a significant spatial pattern.

3.1.3. Carbonate minerals: dolomite and calcite

The $CaCO_3$ concentration was determined with the TGA (Table 1), but it proved impossible to distinguish between the different carbonate minerals due to overlap in the temperature ranges for dolomite and calcite. However, 10 random samples were analysed with the XRD and all were found to contain calcite. Aragonite was not detected in these samples. To explicitly test whether a distinction between dolomite and calcite was possible with the TGA, a test was performed with pure dolomite, calcite and a mixture of the two. Each of these was added to silica sand that contained no carbonate minerals, in order to prevent biased results and to mimic the weight and structure of the sand samples from the field. One specific peak was estimated and as a result it was not possible to distinguish between carbonate minerals using the TGA (see Fig. 2S). Although TGA can be used to distinguish dolomite from calcite, this is difficult, since – as demonstrated by Földvári (2011) – the results depend on the amount of dolomite in the sample, the heating rate, the crystalline structure of dolomite and calcite and the presence of soluble salts. For several samples, the TGA showed very slight slopes to below 550 °C, or a second small peak between 900 and 1000 °C, making it difficult to estimate the appropriate temperature range. The TGA results for carbonates correlate well with the aqua regia Ca concentration (0.88), implying that most Ca in the samples originates from carbonate minerals. The variable $CaCO_3$ was left out of the

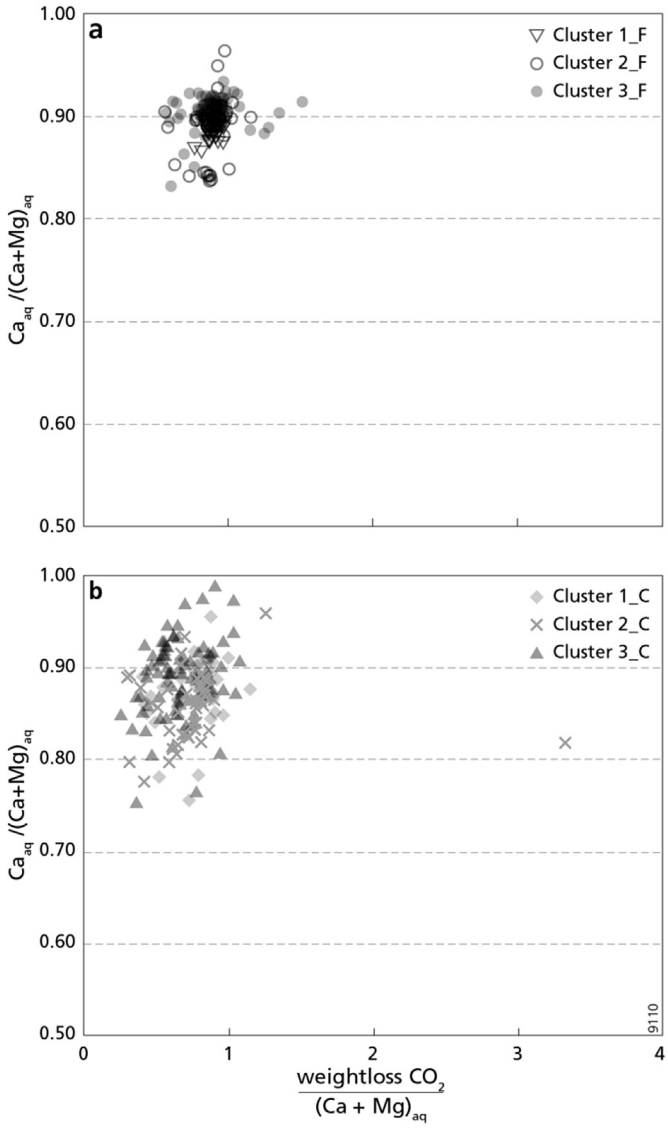

Fig. 3. The ratio of aqua regia ($_{aq}$) concentrations of Ca and Mg where $Ca_{aq}/(Ca + Mg)_{aq}$ is plotted against the ratio of $CO_2/(Ca + Mg)_{aq}$ for the fine fraction (a) and the coarse fraction (b).

statistical analyses to prevent overlap.

To know whether Mg-bearing carbonate minerals (i.e. dolomite or Mg-calcite) are present in the samples, the ratio of Ca/(Ca + Mg) was plotted against the ratio of $CO_2/(Ca + Mg)$, of which the CO_2 is derived from the TGA and the Ca and Mg are aqua regia concentrations (Fig. 3). Magnesium was assumed to be reactive, as estimated from the QR method described in paragraph 3.1. A value of 0.5 for the ratio of Ca/(Ca + Mg) indicates the presence of exclusively dolomite and 1 of only calcite. As all the samples lie between 0.8 and 1, the main component of the $CaCO_3$ minerals is calcite, as expected, but the samples below 1 are varied: they include dolomite, Mg-calcite or even Mg-bearing ankerite. According to Stuyfzand (1993) the average composition of shell fragments in Dutch dune and beach sand is $Sr_{0.002}Na_{0.024}Mg_{0.002}(CaCO_3)_{1.016}(H_2PO_4)_{0.0004}$ where Mg is almost negligible. Therefore, the major source of Mg is most likely not shell fragment related, whereas dissolution of dolomite may be a source.

On the x-axis of Fig. 3 the ratio of $CO_2/(Ca + Mg)$ is around 1 when all the CO_2 weight loss has originated from both Ca and Mg, which is true for most samples, especially for the fine fraction. However, many samples in the coarse fraction are below 1, which may indicate that (1) the TGA has underestimated CO_2 (2) aqua regia Ca and Mg may also originate from silicate minerals, or (3) reactive Fe and Mn are present in the carbonate minerals, including in siderite. One value originated from the BOREHOLE dataset for the coarse fraction was revealed to be an outlier with a ratio of almost 4 where the low concentrations of Ca and Mg do not correspond with the TGA value of CO_2.

When both fractions are compared, the spread of the coarse fraction is larger than that of the fine fraction, which means the variation of Mg- and Ca-bearing minerals is less in the fine fraction. Cluster 1_F of the fine fraction seems to have a lower ratio than the other two clusters, perhaps because of leaching, as dolomite is less vulnerable to leaching (Morse and Arvidson, 2002). Thus it can be concluded that Mg-bearing carbonates like dolomite and Mg-calcite are present in the samples of the dataset, but it is not possible to quantify them with TGA.

3.1.4. Source material

TNO Geological Survey of the Netherlands produced a geological description of some of the samples in the SAND PIT group. The upper layer to an average of 2 m depth was assigned to the Holocene and the deeper parts to the Pleistocene. According to the literature, the fluvial Kreftenheye Formation is present along the Holland coast (Schüttenhelm and Laban, 2005) and most likely in the deeper samples of the SAND PIT group and, as its sand comes from the sand pit, possibly on the Sand Engine. The Kreftenheye Formation, which contains sand and gravel, was predominantly formed during the Late Pleistocene. It is overlain by the Bligh Bank, a member of the Southern Bight Formation (Rijsdijk et al., 2005), which is characterised by sandy marine units that have a high-energy open marine genesis. As a result, Sand Engine material is both fluvial and marine sedimentary in origin and to understand its geochemistry it is necessary to find out whether Sand Engine material can be divided into the two different geological formations. Clusters 2_C and 3_C were described in the previous section. Cluster 2_C has the geochemistry of the SAND PIT samples from depths 1.5–7 m, whereas Cluster 3_C has the geochemistry from depths 0–2 m. Thus the CA shows that there are two different source materials present in the Sand Engine.

Heavy minerals are often used to distinguish between different geological formations (e.g. Baak, 1936; Ludwig and Figge, 1979; Schüttenhelm and Laban, 2005). For the Kreftenheye Formation, the heavy mineral augite is important (Schüttenhelm and Laban, 2005). It is enclosed in the augite-saussurite (AS) association described by Baak (1936) and characterised by the presence of saussurite, garnet, epidote, hornblende and volcanic minerals, including augite, titanite, and dark basaltic hornblende. It is difficult to determine a specific mineralogy for the Bligh Bank member since the samples from the SAND PIT group are nearshore coastal sands and are therefore a mixed group of reworked fluvial and marine deposits (Baak, 1936; Eisma, 1968).

Both Zr and Ti are associated with the heavy mineral fraction, for example as ilmenite, rutile and zircon, of which zircon is most likely to occur in the fine fraction (Moura and Krooneberg, 1990). This is visible in the RFA results, where Zr is included in only one of the three clusters of the coarse fraction. For the fine fraction, both Zr and Ti show up in the RFA results. To illustrate how Zr and Ti behave in relation to Al, the correlations are shown in Fig. 4 for both the fine and coarse fraction. Interestingly, the surface clusters are distinctly different from the other two clusters for both the fine and the coarse fraction. A similar trend is seen in the correlation of both elements with $CaCO_3$. Fig. 4 indicates that more Ti and Zr minerals of the surface clusters were dissolved using the aqua regia method,

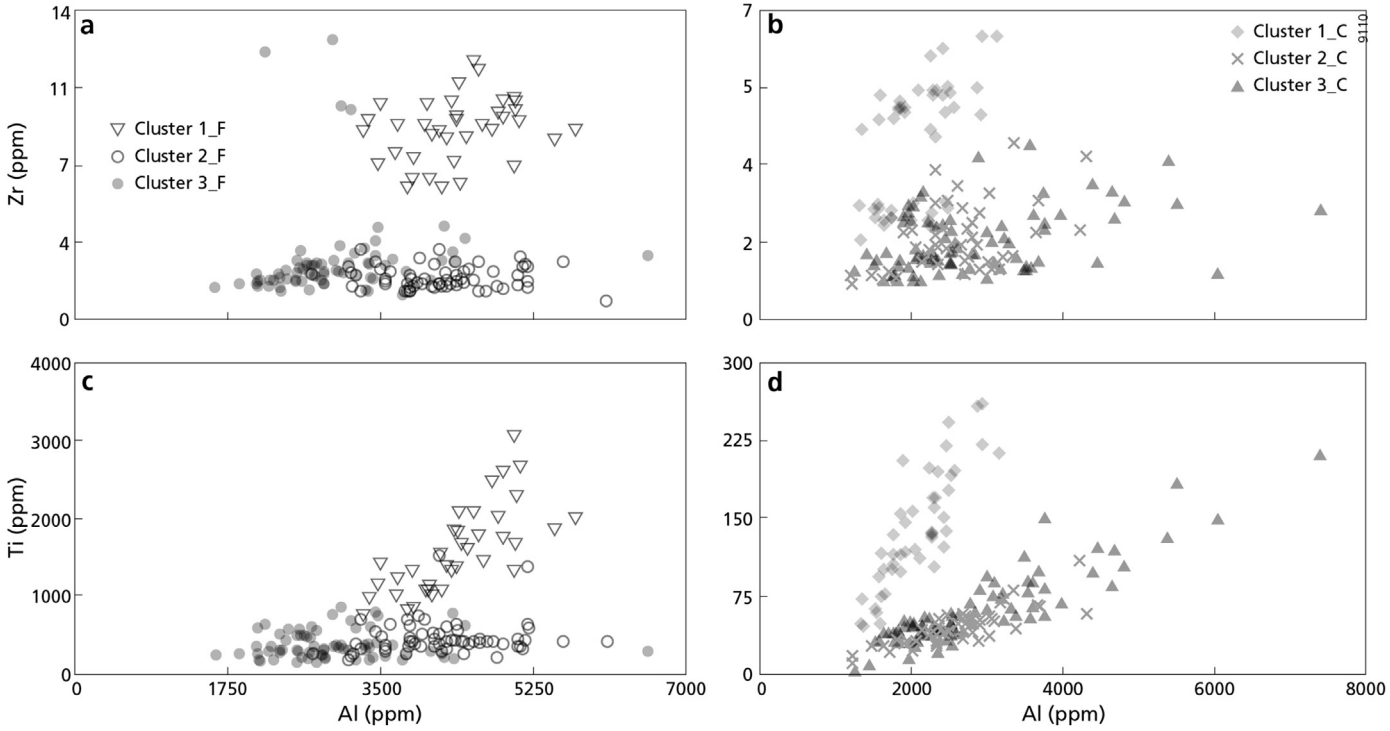

Fig. 4. Correlation between Al, Ti and Zr contents of samples, per cluster, for both the fine fraction (a,c) and the coarse fraction (b,d).

or that the environment of the surface clusters caused Zr and Ti to be increased by comparison with the other clusters. According to Morton and Hallsworth (1999) heavy minerals can be affected by weathering: for example, through mechanical breakdown during transport, or through hydrodynamics. Even though heavy minerals that contain Ti and Zr are considered to be persistent (Morton and Hallsworth, 1999), and therefore in aqua regia solution, the chemistry of the interstitial fluids and particularly the pH can affect the stability of the minerals (Morton, 1984). High-energy environments occur at the surface of the Sand Engine, and this, together with the infiltration of rainwater may have made the heavy minerals less stable and hence easier to dissolve with the aqua regia method. Alternatively, it was not possible to distinguish two geological layers on the basis of elements in our dataset related to heavy minerals.

The majority of the samples contained significant amounts of reactive Fe. Eisma (1968) also found this: the Fe was present as ferric hydroxide coatings, and the average reactive content Fe for the southern Dutch beach sands he investigated was 0.30%, which is slightly lower than the average reactive content Fe of 0.33% we found for the coarse fraction on the Sand Engine. The largest differences for reactive Fe are for Clusters 2 and 3 for both fractions: the coarse fraction shows an average of 0.14% reactive Fe for Cluster 2_C, which is much lower than the average of 0.45% reactive Fe for Cluster 3_C.

As mentioned in section 3.1.1, Cluster 2_C contains deeper samples from the SAND PIT group and Cluster 3_C the shallower samples from the SAND PIT group. Fig. 5 shows reactive Fe versus depth of samples from the SAND PIT group in Clusters 2_C and 3_C. A decreasing trend of reactive Fe is seen where high concentrations are present in the shallow depths between 0 and 3 m; low concentrations are present from 2 to 7 m depth. According to Eisma (1968) this difference may be related to source material. Pleistocene deposits have probably been reduced and therefore may have lost iron, as indicated by their grey colouration (Van Straaten, 1965),

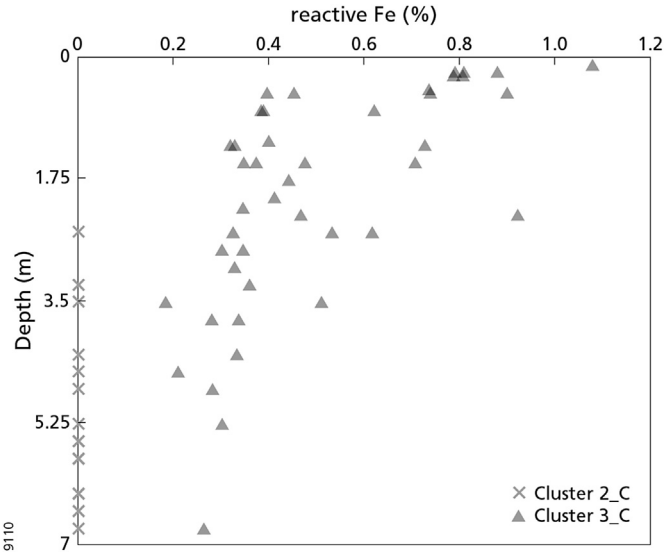

Fig. 5. Reactive Fe content versus depth of samples from the SAND PIT group, for Clusters 2_C and 3_C.

whereas Holocene sediments include recent Rhine sediments that have a high reactive Fe concentration. Recent concentrations of iron in the Rhine-Meuse delta show a range of 0.8–2.2% Fe in the sediment (Canavan et al., 2007), and Dutch governmental monitoring programmes find on average 33 ppm Fe in suspended matter (waterbase.nl). This implies that reactive Fe has been and still is actively entering the North Sea, and may contribute to the differences between the shallow and deep samples of the SAND PIT group. A pattern similar to that of reactive Fe is seen for the elements related to iron, such as As, P, V and Zn (Fig. 6). The correlation

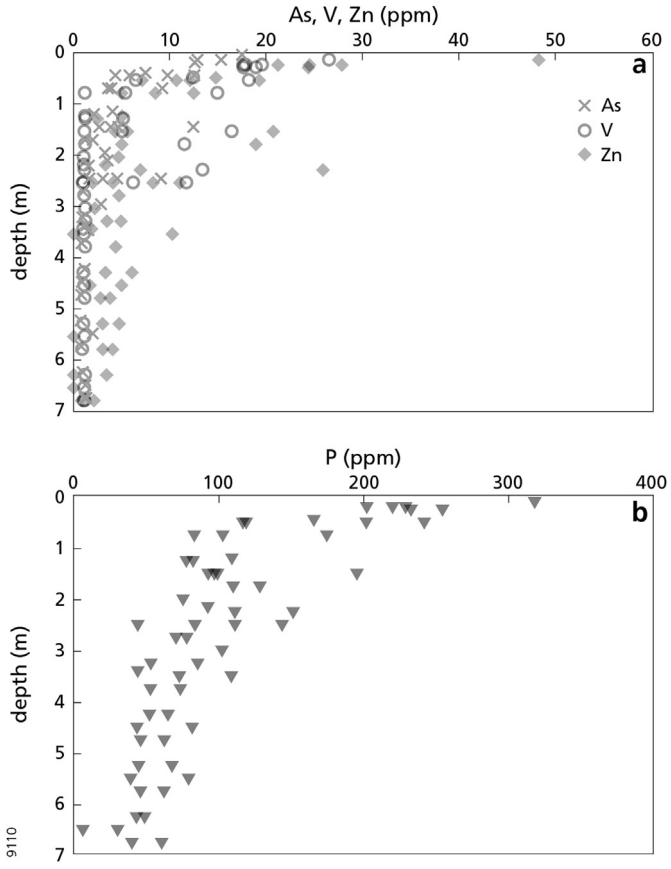

Fig. 6. The aqua regia concentrations of As, V, Zn (a) and P (b) with depth, in samples from the coarse fraction of the SAND PIT group.

between these elements and reactive Fe was shown by the RFA and for the first or second factor of the coarse clusters (Table 3).

As the Sand Engine contains material from Pleistocene and Holocene origin, the mega beach nourishment can be expected to contain a mix of reactive Fe. However, Cluster 1_F has a higher reactive Fe concentration than Cluster 3_F, and Cluster 1_C shows similar concentrations to Cluster 3_C (see Table 1S). It was expected to see more similarities between Cluster 1_C and Cluster 2_C, as Cluster 2_C contains overall shallow samples of the Sand Engine and Cluster 3_C deeper samples. It seems that material from Holocene origin is more dominant at the Sand Engine compared to material from Pleistocene origin. With geological layers not being perfectly horizontal, a maximum depth of 6 m in a sand pit may limit dredging of Pleistocene material. As a result, Cluster 1_C contains a mix of reactive Fe from Pleistocene and Holocene origin, but is dominated with material from Holocene origin and therefore shows a similar concentration of reactive Fe to Cluster 3_C.

3.1.5. Bog iron ore fragments

Bog iron ore fragments are found all over the Sand Engine, mainly on top of it between the C and D transects (see Fig. 1). The fragments are dark brown or reddish brown in colour and range in size from <1 cm to >10 cm. Median concentrations of the main elements are 42.9% Fe, 2.8% Ca, 3476 ppm P and trace element As with a median of 435 ppm. According to Joosten (2004), Dutch bog iron ore typically has high P and As contents. In our study, XRD revealed that the main mineral found in the ores was goethite, although one bog iron ore incorporated a large fraction of pyrite with a concentration of 1.7% S.

Bog iron forms as a result of a change in oxidation state, when ferrous iron is oxidised to ferric iron, resulting in crystalline iron oxyhydroxides (Stanton et al., 2007). Iron-depositing environments include springs and seeps; seeps are likely to have occurred in the sand pit area during the Pleistocene-Holocene transition as the area was terrestrial and peat formation took place when high groundwater tables were present (Busschers et al., 2007; Hijma et al., 2012). The chemistry of the bog iron ore depends on the redox conditions during its growth and on the composition of the groundwater. The presence of the bog iron ores confirms that Pleistocene sediment has been included in the Sand Engine. Small fragments of bog iron ore were visible at the start of this mega beach nourishment, and their number on its surface has increased greatly in the last 3 years. Sorting processes like aeolian activity and sea currents transport the smaller grains of sediment, but fragments of bog iron ore and large shell fragments remain on the surface for a longer period of time until they are broken down (see Fig. 3S). In the coming years it is likely there will be a further relative increase of bog iron ore fragments on the Sand Engine. When these large quantities of bog iron ore fragments weather, the geochemistry of the Sand Engine will change, which may create ecological implications.

Furnace slags were also found. They were not as numerous as bog iron ore fragments, but the fragments were of similar size and the main concentrations of one that was analysed were 3.05% Fe, 1.70% Al, 0.60% Ca, 0.41% K and 0.21% Ti. The source of the slags is unclear. They were probably dumped waste material from steel or cast iron manufacture, as there is are dredging sludge depots of a steel and iron manufacturing area close to the sand pits as seen in Fig. 1 (Dutch Central Government, 2009). The main mineral phases of steel slags are dicalcium silicate, dicalcium ferrite and wustite. The silicates will not dissolve easily with the aqua regia method, which is why we found lower concentrations than those reported in the literature (e.g. Motz and Geiseler, 2001).

3.2. Pore water

A total of 86 pore water samples was used for the CA. Mclust yielded two clusters: see Table 4 for an overview showing the variables plus the means estimated with Mclust, the median, the standard deviation and the maximum for each cluster. The first cluster (Cluster 1_PW) is a saline water cluster that generally has a high sea water content, except for one sample from BH03 at 4.6 m depth with a Cl concentration of 303 ppm. Most of the samples from Cluster 1_PW are from the BOREHOLE group. The second cluster (Cluster 2_PW) is a fresh water cluster, except for one sample from BH03 at 6.4 m depth that has a Cl concentration of 16 585 ppm. This cluster includes shallow samples from the BOREHOLE group and the fresh water samples from the GRID group.

For Cluster 1_PW the RFA resulted in an explained variance of 65% for the first factor, 11% for the second factor, 7% the third factor and 5% for the fourth factor. The number of factors used for the RFA was checked with a scree plot (Reimann et al., 2008) and with four factors at least 70% of the variety was explained. The significant positive loadings for the first factor shows the presence of saline water with significant positive loadings for Mg, Na, Cl, Ca, K, SO_4 and pH. The significant negative loadings are Mn, Fe, P and As and may contribute to redox processes. However, with important variables like NO_3 and Br excluded from the RFA, it was not possible to interpret oxidation and reduction processes or cation exchange due to freshening or saltwater intrusion, based on RFA alone. Additionally, it was expected that HCO_3 would be classified as a significant loading, but this did not occur. The same holds for Cluster 2_PW, where the first factor explains 34% of the variance, the

Table 4
The distribution of the samples of each cluster estimated by Mclust from the sample groups GRID and BOREHOLE, together with the results of the cluster analysis: Clusters 1_PW and 2_PW with the median, standard deviation (stdev), maximum value in ppm, and with the estimated means from the Mclust.

	Cluster 1_PW				Cluster 2_PW			
from GRID (n)	16				24			
from BOREHOLE (n)	34				12			
	median (ppm)	stdev (ppm)	max (ppm)	Mclust means	median (ppm)	stdev (ppm)	max (ppm)	Mclust means
Al	0.01	0.08	0.55	−0.15	0.02	0.04	0.17	0.21
As	0.01	0.02	0.10	0.13	0.005	0.008	0.031	−0.18
Ca	393	125	764	0.71	31	91	389	−0.98
Cl	15 178	4147	19 883	0.75	226	2931	16,585	−1.05
Co	0.0003	0.004	0.03	0.30	0.0002	0.0004	0.0021	−0.42
Cu	0.01	0.01	0.06	−0.07	0.01	0.01	0.05	0.09
Fe	1.40	3.66	15.20	0.46	0.02	0.16	0.70	−0.64
HCO_3	276	147	669	0.21	255	167	889	−0.29
K	292	81	384	0.73	36	68	336	−1.02
Mg	974	276	1232	0.76	22	219	1038	−1.05
Mn	0.93	1.25	4.88	0.56	0.005	0.158	0.835	−0.78
Na	8732	2311	11 140	0.75	272	1920	9164	−1.04
Ni	0.002	0.006	0.025	−0.02	0.002	0.008	0.045	0.03
P	0.19	1.12	6.20	0.18	0.10	0.27	1.14	−0.26
pH	7.61	0.32	8.47	−0.67	8.35	0.33	8.77	0.93
Sb	0.0005	0.0005	0.003	−0.44	0.001	0.001	0.005	0.61
SO_4	1907	485	2677	0.78	129	361	1995	−1.08
V	0.002	0.003	0.022	−0.32	0.005	0.007	0.035	0.44
Zn	0.01	0.14	0.97	0.13	0.005	0.01	0.09	−0.18

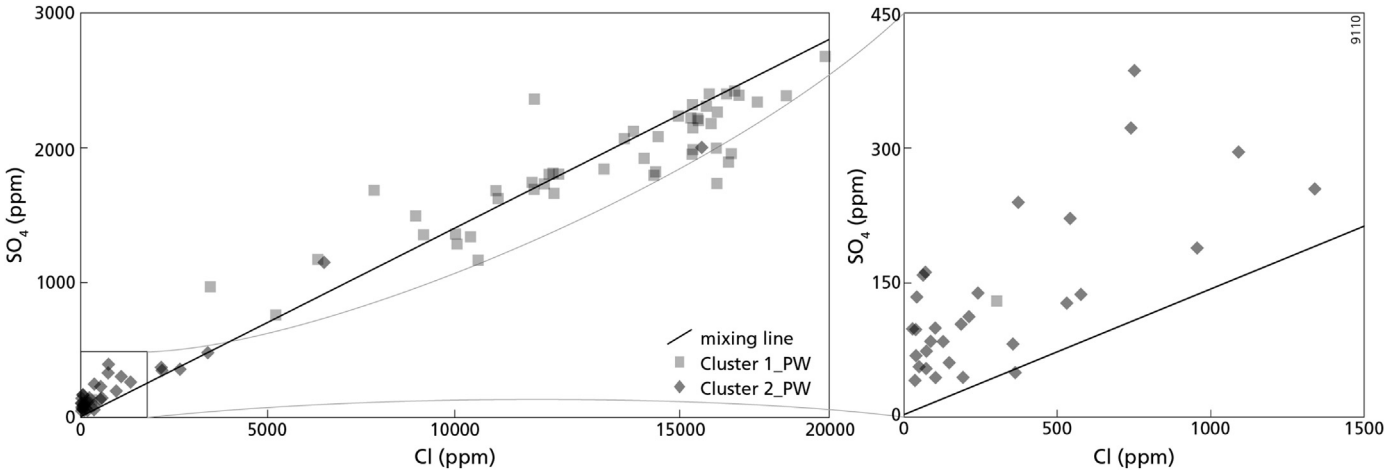

Fig. 7. The concentrations of SO_4 and Cl for groundwater samples at the Sand Engine, including a close-up (right panel) and the mixing line of fresh water and sea water.

second factor 18%, the third factor 13%, and the fourth factor 7%. Further interpretation is therefore performed on basis of hydrochemical processes instead of statistical results.

3.2.1. Pyrite

To estimate whether pyrite oxidation has occurred in the Sand Engine, the amount of excess sulphate was calculated similar to the way freshening is calculated using equations (1)–(3) (Fig. 7). Concentrations of Cl determine the main groundwater types, which we divided into fresh (<150 ppm Cl), fresh-brackish (150–300 ppm Cl), brackish (300–1000 ppm Cl), brackish-saline (1000–10 000 ppm Cl) and saline (10 000–20 000 ppm Cl) (Stuyfzand, 1986). Excess values of SO_4 are primarily visible for Cluster 2_PW in fresh to brackish water samples with values from 39 to 385 ppm. In brackish to brackish-salt samples in Cluster 1_PW, values of SO_4 excess are high: from 129 to 1684 ppm, whereas the saline samples show low SO_4 excess values from −616 to 142 ppm and are often below the mixing line, indicating SO_4 reduction.

Fig. 8 contains samples from BH07 and BH08 to show values for excess SO_4 and Cl concentrations with depth below mean sea level. Positive SO_4 excess values suggest pyrite oxidation and negative values SO_4 reduction. Both boreholes show a similar pattern for the Cl concentration: between 2 and 4 m below mean sea level the water goes from fresh to saline, and both boreholes decrease in Cl concentration at the depth of nourishment material. As described above, BH07 contains material below the nourishment, which starts at a depth of around 9 m below mean sea level; for BH08 this depth is at around 5 m below mean sea level. A mixture of groundwater flow from the dunes and old water from the river Rhine may have altered the Cl concentration at depth in BH07 and BH08 (Stuyfzand et al., 2012a).

With pyrite oxidation in the shallow part of the boreholes and SO_4 reduction at greater depths, sedimentary S concentrations are expected to increase with depth. Fig. 9 shows the sedimentary S concentrations from the boreholes for the coarse and fine fractions. Overall, sulphur concentrations are low until a depth of around 6 m

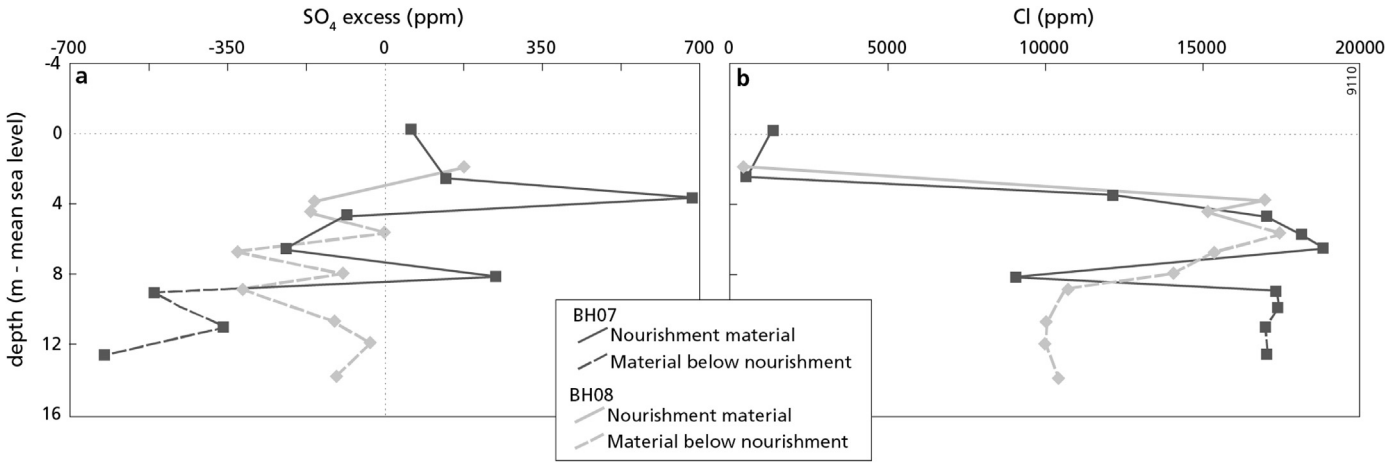

Fig. 8. Pore water samples from BH07 and BH08 to show SO_4 excess values and Cl concentrations with depth below mean sea level.

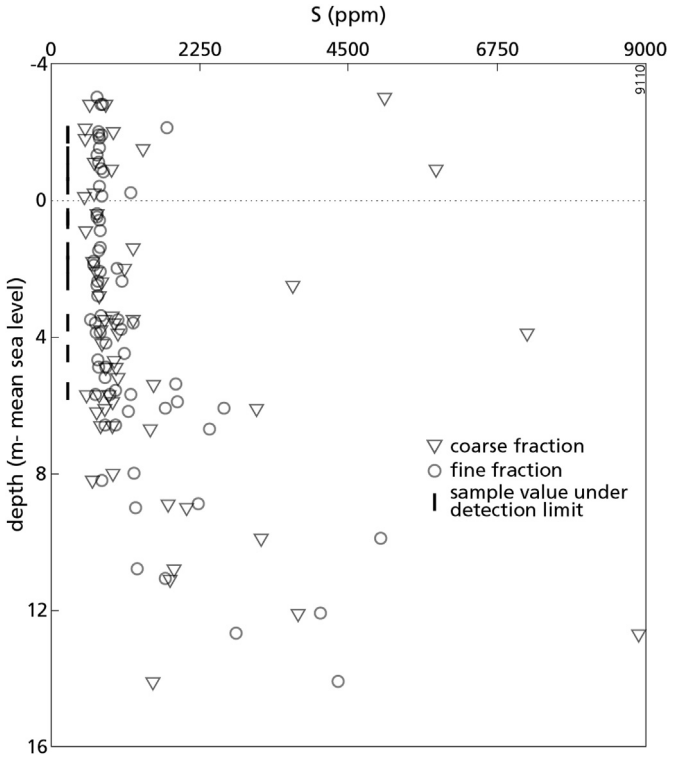

Fig. 9. Sedimentary S concentrations of all borehole samples for the coarse and fine fractions.

below mean sea level, with a median concentration of 727 ppm S for the coarse fraction and of 748 ppm S for the fine fraction. From 6 to 14 m below mean sea level, both fractions increase in sedimentary S concentration, with a median concentration of 1655 ppm S for the coarse fraction and of 1730 ppm S for the fine fraction. The increase of sedimentary S coincides well with the bottom of the mega beach nourishment, where material prior to the mega beach nourishment starts to be found. Four shallow borehole samples show high sedimentary S, which is not related to the presence of clay or silt but may be related to incidental higher S contents in parent material. To confirm the existence of pyrite at the Sand Engine, sediment samples with relatively high S concentrations were studied with the tabletop SEM. Only framboidal pyrite was found: an example is shown in Fig. 4S. Sedimentary S concentrations in the samples of the SAND PIT group are not significantly higher compared to the GRID group samples. Therefore, the source material of the Sand Engine contains overall a low amount of S minerals.

It can therefore be concluded from the fresh to brackish-salt samples that pyrite oxidation is present at the Sand Engine and that in saline waters SO_4 reduction is dominant. Sedimentary S concentrations are rather low until a depth of around 6 m below mean sea level, where material below the mega beach nourishment has more abundant S minerals.

3.2.2. Cation exchange

Freshening induces cation exchange where Ca^{2+} from fresh water exchanges with Na^{+}, K^{+} and Mg^{2+} from the cation exchange complex in a sea water aquifer (Appelo and Postma, 2005). The chemical reactions occurring during freshening can be elucidated by comparing the measured water composition with the composition for conservative mixing of fresh water and sea water. Fig. 10 shows the concentrations of Na, Ca, Mg and K with Cl, where concentrations above the mixing line of fresh water and sea water indicates enrichment and concentrations below the mixing line shows depletion compared to plain mixing. Additionally, the standard deviation has been added in Fig. 10, in order to highlight possible analytical errors instead of a hydrochemical process.

Fig. 10a shows that most of the fresh water samples are above the mixing line. Those below the mixing line all come from the southern part of transect A (see Fig. 1). This may be because of the presence of a small lake, which is located close to these samples and has a Cl concentration of 6014 ppm. Given that the lake is 4 m deep, intrusion of diluted salt water may have resulted in depletion of Na in the southern samples of transect A. Further, depletion of Na can be expected if Cl concentration increases, but some samples with high Cl concentrations show freshening processes. These samples are located above the mixing line and indicate enrichment of Na. According to Griffioen (2003), freshening can be present in saline water when this water is replacing more saline groundwater. This is true for the deeper samples from BH07 and BH08, where lower concentrations of Cl are present than in sea water; as a result of cation exchange, these samples are located above the mixing line.

For K (Fig. 10b), a clear distinction is visible between the fresh and brackish water samples (with Cl concentrations from 0 to 10 000 ppm) and the salt water samples (with Cl concentrations of >10 000 ppm). Three samples containing about 10 000 ppm Cl

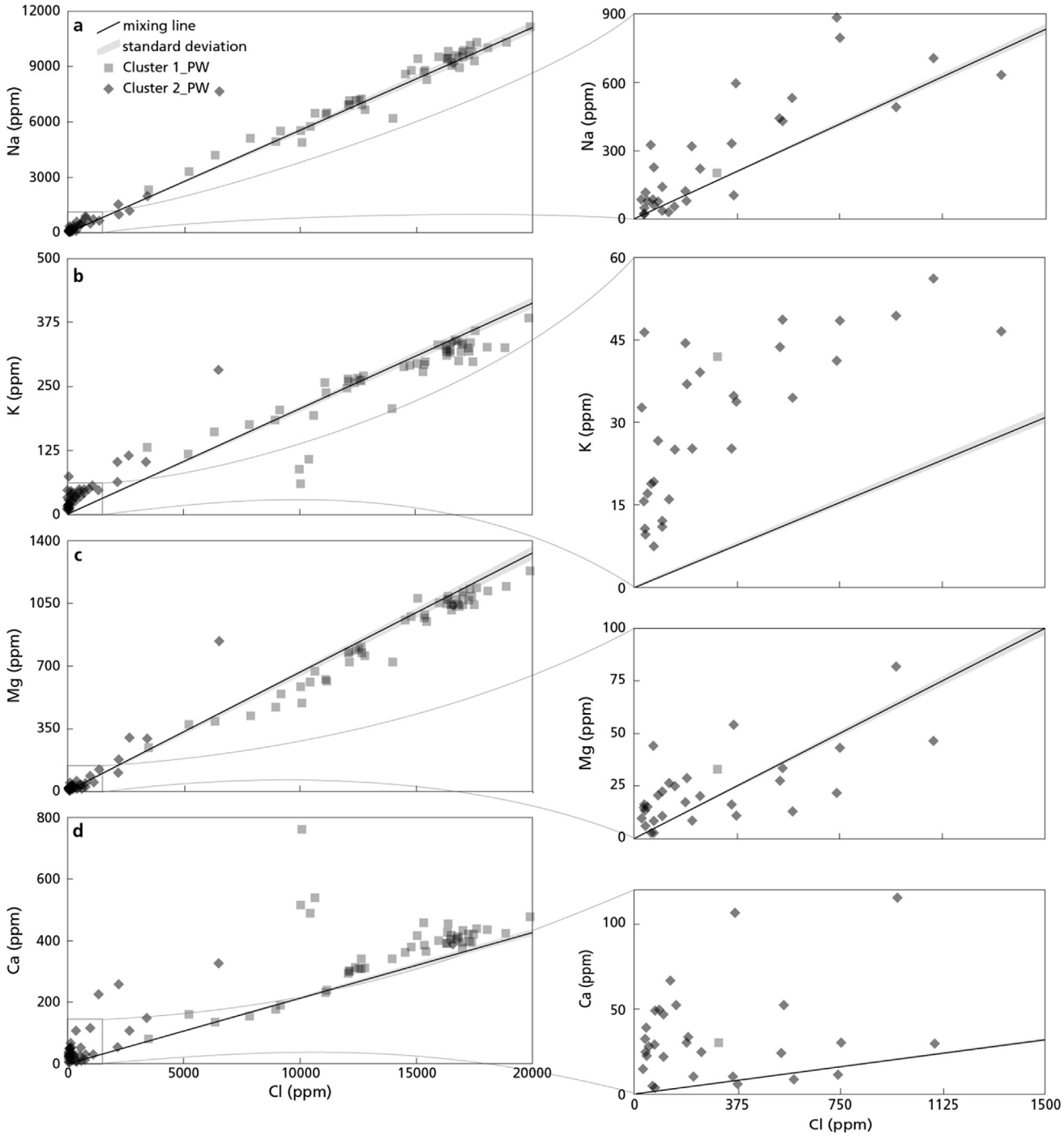

Fig. 10. The concentrations of Na, K, Mg and Ca against Cl, and a mixing line of fresh water and sea water. (Close-ups on the right).

show a large depletion: all are from the deepest depths of BH08. For Mg (Fig. 10c), the majority of the fresh water samples are above the mixing line and show enrichment, probably as a result of cation exchange. Depletion of Mg becomes dominant when Cl concentration increases. For the brackish-saline water samples where dilution of sea water is present through fresh water intrusion, Mg shows the highest affinity for the exchanger (Griffioen, 2003). This implies that depletion of Mg occurs in the zone where fresh and saline water mix. When Cl concentrations are close to sea water concentrations, Na is favoured on the exchanger.

Enrichment of Ca is seen for almost all the samples (Fig. 10d). No fluctuations in Ca caused by cation exchange are present. Thus, in addition to cation exchange, Ca seems to be increased by processes like pyrite oxidation and acid production where calcite has dissolved, thereby increasing the Ca concentration. The sea water Cluster 1_PW contains a calcite Saturation Index (SI) ranging from −0.41 to 0.94; in Cluster 2_PW the SI ranges from −0.90 to 1.08. The strongly negative SI values that show undersaturation are seen for samples from the BOREHOLE group from depths between 3.4 and 3.9 m below mean sea level where Cl concentrations are

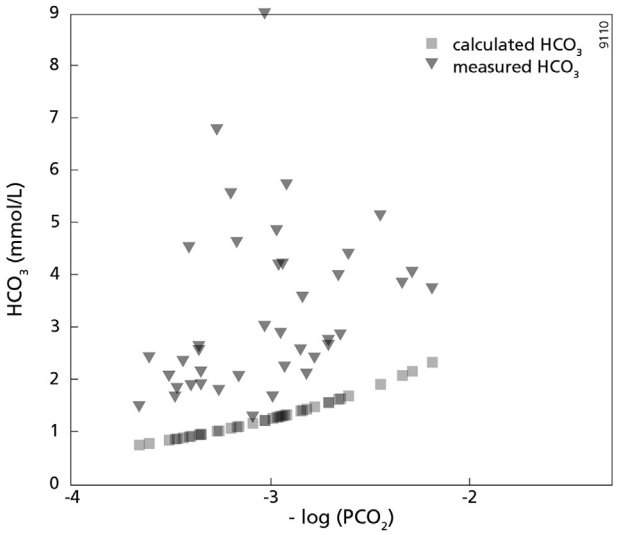

Fig. 11. The expected HCO_3^- concentration resulting from carbonate dissolution was calculated and plotted with the measured HCO_3^- concentrations of samples from the GRID group.

high (around 16 000 ppm Cl). As a result, Ca itself is not an appropriate measure for Ca adsorption or desorption caused by freshening (Appelo, 1994; Griffioen, 2003).

Using the CO_2 partial pressure, the expected HCO_3^- concentration resulting from carbonate dissolution was calculated for the samples from the GRID group. The pore water samples from the GRID group were sampled at 50 cm depth, which is probably in contact with the atmosphere and therefore close to an open CO_2 system. Fig. 11 shows the calculated and measured HCO_3^- concentrations of the water samples from the GRID group. The measured HCO_3^- concentrations are all higher than the calculated HCO_3^- concentrations. The difference between the measured and calculated HCO_3^- shows that the alkalinity cannot be explained by calcite dissolution in an open CO_2 system. The enrichment in alkalinity brings forward that additional processes like pyrite oxidation and calcite dissolution resulting from cation exchange are causing the alkalinity to rise.

4. Conclusions

The objective of this study was to statistically determine the geochemistry of the Sand Engine pilot project and to understand the compositional changes of the material used to build the Sand Engine, with respect to pyrite oxidation and freshening, as well as to grain size distribution. The CA performed with model-based clustering resulted in three clusters for both the fine 0–150 μm fraction and the coarse 150–2000 μm fraction. The samples from the Sand Engine were divided into cluster 1 (exclusively surface samples), cluster 2 (shallow samples) and cluster 3 (deep samples). The RFA revealed carbonate minerals to be the dominant reactive minerals in the Sand Engine. A significant difference between cluster 1 vis-à-vis clusters 2 and 3 is the concentration of the heavy mineral related elements Zr and Ti. In cluster 1 these two elements have higher concentrations and correlate differently with Al on the surface of the Sand Engine than is the case for the other two clusters. These differences are presumably related to weathering processes, which are more intensively present at the surface of the Sand Engine, and may have caused the heavy mineral related elements Ti and Zr to dissolve more in the aqua regia method used for this study. The difference between clusters 2 and 3 is source-related: cluster 2 contains Pleistocene material and cluster 3 Holocene material from the sand pit. As a consequence of dredging, the Sand Engine contains the two different geological layers from the sand pit, but these have been inverted. The significant difference between clusters 2 and 3 is the concentration of reactive Fe, which is much higher in cluster 3 than in cluster 2. The distribution of reactive Fe seems to be related to pyrite oxidation, paleohydrological diagenesis source material and sorting processes. The presence of S minerals is apparent, but concentrations are low. Excess sulphate was found in the pore waters to the depth of the mega beach nourishment, indicating that pyrite oxidation is present at depth in the Sand Engine. Below the mega beach nourishment, higher S concentrations are present in the sediment and excess sulphate values become negative for groundwater, indicating SO_4 reduction. The pore water dataset resulted in two clusters with model-based clustering: a fresh water cluster and a saline water cluster. The pore water data shows that cation exchange as a result of freshening, as well as pyrite oxidation is altering the geochemistry of the Sand Engine. Related carbonate dissolution is increasing the alkalinity as well as the Ca concentration. With the Sand Engine having a low amount of sulphide minerals, the mega beach nourishment becomes most likely 'flushed' with respect to pyrite, because of the calculated pyrite oxidation based on SO_4 excess. Source material is therefore expected to show a decrease in pyrite oxidation with the development of the Sand Engine. Carbonate dissolution as a consequence of pyrite oxidation will then decrease as well. With the amount of $CaCO_3$ present in the sand at the Sand Engine, pyrite oxidation and cation exchange will most likely not cause local environmental impacts due to acidification.

Acknowledgements

This research was supported by NatureCoast, a project of Technology Foundation STW, applied science division of the Netherlands Organisation for Scientific Research (NWO). The authors would like to thank Sytze van Heteren, Bram Hoogendoorn and Isabel Trujillo Rocha for advice and support on the field campaign. Constructive comments from the two reviewers are gratefully acknowledged as they have contributed to improve the manuscript.

Appendix A. Supplementary data

Supplementary data related to this article can be found at http://dx.doi.org/10.1016/j.apgeochem.2017.02.003.

References

Acosta, J.A., Martínez-Martínez, S., Faz, A., Arocena, J., 2011. Accumulations of major and trace elements in particle size fractions of soils on eight different parent materials. Geoderma 161, 30–42. http://dx.doi.org/10.1016/j.geoderma.2010.12.001.

Aitchison, J., 1982. The statistical analysis of compositional data. J. R. Stat. Soc. Ser. B. Methodol. 44, 139–177. http://dx.doi.org/10.2307/2345821.

Appelo, C.A., Postma, D., 2005. Geochemistry, Groundwater and Pollution, second ed. A.A. Balkema Publishers, Leiden, The Netherlands.

Appelo, C.A.J., 1994. Cation and proton exchange, pH variations, and carbonate reactions in a freshening aquifer. Water Resour. Res. 30, 2793–2805. http://dx.doi.org/10.1029/94WR01048.

Appelo, C.A.J., Verweij, E., Schäfer, H., 1998. A hydrogeochemical transport model for an oxidation experiment with pyrite/calcite/exchangers/organic matter containing sand. Appl. Geochem. 13, 257–268. http://dx.doi.org/10.1016/S0883-2927(97)00070-X.

Baak, J.A., 1936. Regional Petrology of the Southern North Sea. Ph.D-thesis. Leiden University, The Netherlands, 127pp.

Bakker, M.A.J., van Heteren, S., Vonhögen, L.M., van der Spek, A.J.F., van der Valk, B., 2012. Recent coastal dune development: effects of sand nourishments. J. Coast. Res. 282, 587–601. http://dx.doi.org/10.2112/JCOASTRES-D-11-00097.1.

Boggs, S., 2009. Petrology of Sedimentary Rocks. Cambridge University Press, 600 pp.

Busschers, F.S., Kasse, C., Van Balen, R.T., Vandenberghe, J., Cohen, K.M., Weerts, H.J.T., Wallinga, J., Johns, C., Cleveringa, P., Bunnik, F.P.M., 2007. Late Pleistocene evolution of the Rhine–Meuse system in the southern North Sea basin: imprints of climate change, sea-level oscillation and glacioisostacy. Quat. Sci. Rev. 26, 3216–3248. http://dx.doi.org/10.1016/j.quascirev.2007.07.013.

Canavan, R.W., Van Cappellen, P., Zwolsman, J.J.G., van den Berg, G.A., Slomp, C.P., 2007. Geochemistry of trace metals in a fresh water sediment: field results and diagenetic modeling. Sci. Total Environ. 381, 263–279. http://dx.doi.org/10.1016/j.scitotenv.2007.04.001.

Cantwell, M.G., Burgess, R.M., King, J.W., 2008. Resuspension of contaminated field and formulated reference sediments. Part I: evaluation of metal release under controlled laboratory conditions. Chemosphere 73 (11), 1824–1831.

Chen, M., Ma, L.Q., 2001. Comparison of three aqua regia digestion methods for twenty Florida soils. Soil Sci. Soc. Am. J. 65, 491. http://dx.doi.org/10.2136/sssaj2001.652491x.

De Ruig, J.H.M., 1998. Coastline management in The Netherlands: human use versus natural dynamics. J. Coast. Conserv. 4, 127–134. http://dx.doi.org/10.1007/BF02806504.

De Vriend, H.J., Van Koningsveld, M., 2012. Building with Nature: Thinking, Acting and Interacting Differently. Ecoshape, Dordrecht, The Netherlands. http://dx.doi.org/10.1080/02513625.2014.925714.

Dellwig, O., Watermann, F., Brumsack, H.J., Gerdes, G., 1999. High-resolution reconstruction of a Holocene coastal sequence (NW Germany) using inorganic geochemical data and diatom inventories. Estuar. Coast. Shelf Sci. 48, 617–633. http://dx.doi.org/10.1006/ecss.1998.0462.

Dutch Central Government, 2009. Policy Document on the North Sea 2009-2015 (The Hague, The Netherlands).

Egozcue, J.J., Pawlowsky-Glahn, V., Mateu-Figueras, G., Barceló-Vidal, C., 2003. Isometric logratio transformations for compositional data analysis. Math. Geol. 35, 279–300. http://dx.doi.org/10.1023/A:1023818214614.

Eisma, D., 1968. Composition, origin and distribution of Dutch coastal sands between Hoek van Holland and the island of Vlieland. Neth. J. Sea Res. 4, 123–267.

Filzmoser, P., Hron, K., Reimann, C., 2009. Univariate statistical analysis of environmental (compositional) data: problems and possibilities. Sci. Total Environ. 407, 6100–6108. http://dx.doi.org/10.1016/j.scitotenv.2009.08.008.

Fiselier, J., 2010. Projectnota/MER, Aanleg en zandwinning Zand motor Delflandse kust (Sand Engine Delfland coast: project plan and assessment of the environmental impact report). DHV BV. Amersfoort, The Netherlands.

Földvári, M., 2011. Handbook of Thermogravimetric System of Minerals and its Use in Geological Practice, first ed. Geological Institute of Hungary, Hungary.

Greene, K., 2002. Bethesda. Beach Nourishment: a Review of the Biological and Physical Impacts by Fish, vol. 1, pp. 155–161. http://dx.doi.org/10.1007/BF02463334.

Griffioen, J., 2003. Kation-uitwisselingspatronen bij zoet/zout grondwaterverplaatsingen (in Dutch). Stromingen 9.

Griffioen, J., Klaver, G., Westerhoff, W.E., 2016. The mineralogy of suspended matter, fresh and Cenozoic sediments in the fluvio-deltaic Rhine–Meuse–Scheldt–Ems area, The Netherlands: an overview and review. Neth. J. Geosci. 95, 23–107.

Hamm, L., Capobianco, M., Dette, H.H., Lechuga, A., Spanhoff, R., Stive, M.J.F., 2002. A summary of European experience with shore nourishment. Coast. Eng. 47, 237–264. http://dx.doi.org/10.1016/S0378-3839(02)00127-8.

Hanson, H., Brampton, A., Capobianco, M., Dette, H.H., Hamm, L., Laustrup, C., Lechuga, A., Spanhoff, R., 2002. Beach nourishment projects, practices, and objectives - a European overview. Coast. Eng. 47, 81–111. http://dx.doi.org/10.1016/S0378-3839(02)00122-9.

Heerdink, R., Griffioen, J., 2008. Methodeontwikkeling voor het berekenen van het gehalte reactief ijzer uit totaalgehaltes ijzer en aluminium in sediment (in Dutch). TNO Geological Survey of the Netherlands. Utrecht, report no. 2008-U-R1278/A.

Hijma, M.P., Cohen, K.M., Roebroeks, W., Westerhoff, W.E., Busschers, F.S., 2012. Pleistocene Rhine–Thames landscapes: geological background for hominin occupation of the southern North Sea region. J. Quat. Sci. 27, 17–39.

Hillyer, T.M., 1996. Shoreline Protection and Beach Erosion Control Study. Final Report: An Analysis of the U.S. Army Corps of Engineers Shore Protection Program. IWR Report 96-PS-1. U.S. Army Corps of Engineers.

Houba, V.J.G., Van der Lee, J.J., Novozamsky, I., 1995. Soil and Plant Analysis. Part 5B Soil Analysis Procedures, 6th ed. Dep. Soil Sci. and Plant Nutr., Wageningen Agricultural University.

Houghton, K.J., Vafeidis, A.T., Neumann, B., Proelss, A., 2010. Maritime boundaries in a rising sea. Nat. Geosci. 3, 813–816. http://dx.doi.org/10.1038/ngeo1029.

Huerta-Diaz, M.A., Morse, J.W., 1990. A quantitative method for determination of trace metal concentrations in sedimentary pyrite. Mar. Chem. 29, 119–144.

Huisman, D.J., 1998. Geochemical Characterization of Subsurface Sediments in the Netherlands. Ph.D-thesis. Wageningen University, The Netherlands.

Huisman, D.J., Kiden, P., 1998. A geochemical record of Late Cenozoic sedimentation history in the southern Netherlands. Geol.. Mijnb 76, 277–292.

Ihaka, R., Gentleman, R., 1996. R: a language for data analysis and graphics. J. Comput. Graph. Stat. 5, 299–314.

IPCC, 2014. Climate Change 2014: Synthesis Report. Contribution of Working Groups I, II and III to the Fifth Assessment Report of the Intergovernmental Panel on Climate Change. Core Writing Team, R.K. Pachauri and L.A. Meyer. IPCC. http://dx.doi.org/10.1017/CBO9781107415324.004.

Joosten, 2004. Technology of Early Historical Iron Production in the Netherlands. Ph.D-thesis. Free University, The Netherlands.

Kabat, P., Fresco, L.O., Stive, M.J.F., Veerman, C.P., Van Alphen, J.S.L.J., Parmet, B.W.A.H., Hazeleger, W., Katsman, C.A., 2009. Dutch coasts in transition. Nat. Publ. Gr 2. http://dx.doi.org/10.1038/ngeo572.

Laursen, S., 1991. On gaseous diffusion of CO2 in the unsaturated zone. J. hydrology 122 (1–4), 61–69.

Lindeman, K., 69 others, 2000. "RE: 70 Ph.D. Scientists Urge Higher Environmental Standards in Beach Dredge and Fill Projects," letter to Colonel Joe Miller. District Engineer, Jacksonville District, U.S. Army Corps of Engineers, 5p.

Liu, N., Chen, H., Shu, L., Zong, R., Yao, B., Statheropoulos, M., 2004. Gaussian smoothing strategy of thermogravimetric data of biomass materials in an air atmosphere. Ind. Eng. Chem. Res. 43, 4087–4096. http://dx.doi.org/10.1021/ie049932s.

Ludwig, G., Figge, K., 1979. Schwermineralvorkommen und Sandverteilungin der deutschen Bucht. (Heavy mineral occurrences and sand distribution in the German Bight). Geol. Jahrb. 32, 23–68.

McLachlan, A., 1996. Physical factors in benthic ecology: effects of changing sand particle size on beach fauna. Mar. Ecol. Prog. Ser. http://dx.doi.org/10.3354/meps131205.

Mengel, M., Levermann, A., Frieler, K., Robinson, A., Marzeion, B., Winkelmann, R., 2016. Future sea level rise constrained by observations and long-term commitment. Proc. Natl. Acad. Sci. 113 (10), 2597–2602. http://dx.doi.org/10.1073/pnas.1500515113.

Moore, D.S., McCabe, G.P., 1989. Introduction to the Practice of Statistics. WH Freeman/Times Books/Henry Holt & Co.

Morse, J.W., Arvidson, R.S., 2002. The dissolution kinetics of major sedimentary carbonate minerals. Earth-Science Rev. 58, 51–84.

Morton, A.C., 1984. Stability of detrital heavy tertiary sandstones from sea basin minerals in the north. Clay Min. 19, 287–308.

Morton, A.C., Hallsworth, C.R., 1999. Processes controlling the composition of heavy mineral assemblages in sandstones. Sediment. Geol. 124, 3–29. http://dx.doi.org/10.1016/S0037-0738(98)00118-3.

Motz, H., Geiseler, J., 2001. Products of steel slags an opportunity to save natural resources. In: Waste Management. http://dx.doi.org/10.1016/S0956-053X(00)00102-1.

Moura, M.L., Krooneberg, S.B., 1990. Geochemistry of Quaternary fluvial and eolian sediments in the southeastern Netherlands. Geol.. Mijnb 69, 359–373.

Mulder, J.P.M., Tonnon, P.K., 2011. "Sand engine": Background and design of a mega-nourishment pilot in the netherlands. Proceedings of the 32nd International Conference on Coastal Engineering, Shanghai, China.

Nel, R., Campbell, E.E., Harris, L., Hauser, L., Schoeman, D.S., McLachlan, A., du Preez, D.R., Bezuidenhout, K., Schlacher, T.A., 2014. The status of sandy beach science: past trends, progress, and possible futures. Estuar. Coast. Shelf Sci. http://dx.doi.org/10.1016/j.ecss.2014.07.016.

Nelson, W.G., 1993. Beach restoration in the southeastern US: environmental effects and biological monitoring. Ocean. Coast. Manag. 19, 157–182. http://dx.doi.org/10.1016/0964-5691(93)90004-I.

Nordstrom, K.F., 2014. Living with shore protection structures: a review. Estuar. Coast. Shelf Sci. http://dx.doi.org/10.1016/j.ecss.2013.11.003.

Parkhurst, D.L., Appelo, C., 2013. Description of Input and Examples for PHREEQC Version 3 — A Computer Program for Speciation, Batch-Reaction, One-Dimensional Transport, and Inverse Geochemical Calculations. U.S. Geological Survey Techniques and Methods, book 6, chapter A43, 497 p. U.S. Geol. Surv. Tech. Methods, B. 6, chapter A43 6–43A.http://dx.doi.org/10.1016/0029-6554(94)90020-5.

Phua, C., Van den Akker, S., Baretta, M., Van Dalfsen, J., 2002. Ecological Effects of Sand Extraction in the North Sea. Stichting De Noordzee, Utrecht.

Pye, K., Blott, S.J., 2004. Comparison of soils and sediments using major and trace element data. Geol. Soc. Lond. Spec. Publ. 232, 183–196. http://dx.doi.org/10.1144/GSL.SP.2004.232.01.17.

Reimann, C., Filzmoser, P., Garrett, R., Dutter, R., 2008. Statistical Data Analysis Explained: Applied Environmental Statistics with R, vol. 2008. Wiley, Chichester, UK, 343 pp.

Rijkswaterstaat, 1990. A New Coastal Defence Policy for the Netherlands. Dutch Ministry of Transport and Public Works Policy Report (The Hague, The Netherlands).

Rijsdijk, K.F., Passchier, S., Weerts, H.J.T., Laban, C., van Leeuwen, R.J.W., Ebbing, J.H.J., 2005. Revised Upper Cenozoic stratigraphy of the Dutch sector of the North Sea Basin: towards an integrated lithostratigraphic, seismostratigraphic and allostratigraphic approach. Neth. J. Geosciences - Geol. en Mijnb 84, 129–146.

Russak, A., Sivan, O., 2010. Hydrogeochemical tool to identify salinization or freshening of coastal aquifers determined from combined field work, experiments, and modeling. Environ. Sci. Technol. 44, 4096–4102. http://dx.doi.org/10.1021/es1003439.

Sanford, W.E., Konikow, L.F., 1989. Simulation of calcite dissolution and porosity changes in saltwater mixing zones in coastal aquifers. Water Resour. Res. http://dx.doi.org/10.1029/WR025i004p00655.

Saye, S.E., Pye, K., 2006. Variations in chemical composition and particle size of dune sediments along the west coast of Jutland. Den. Sed. Geol. http://dx.doi.org/10.1016/j.sedgeo.2005.09.011.

Schokker, J., Cleveringa, P., Murray, A.S., Wallinga, J., Westerhoff, W.E., 2005. An OSL dated middle and late quaternary sedimentary record in the Roer Valley Graben (southeastern Netherlands). Quat. Sci. Rev. 24 (20), 2243–2264.

Schüttenhelm, R.T.E., Laban, C., 2005. Heavy minerals, provenance and large scale dynamics of seabed sands in the Southern North Sea: Baak's (1936) heavy mineral study revisited. Quat. Int. http://dx.doi.org/10.1016/j.quaint.2004.10.012.

Seeberg-Elverfeldt, J., Schlüter, M., Feseker, T., Kölling, M., 2005. Rhizon sampling of pore waters near the sediment/water interface of aquatic systems. Limnol. Oceanogr. Methods 3 (8), 361–371.

Smits, A.J.M., Nienhuis, P.H., Saeijs, H.L.F., 2006. Changing estuaries, changing views. Hydrobiologia 565 (1), 339–355. http://dx.doi.org/10.1007/s10750-005-1924-4.

Stanton, M., Yager, D., Fey, D., Wright, W., 2007. Formation and geochemical significance of iron bog deposits. Integr. Investig. Environ. Eff. Hist. Min. Animas River Watershed, S. Juan. Cty. Color 693–718.

Stive, M.J.F., De Schipper, M.A., Luijendijk, A.P., Aarninkhof, S.G.J., Van Gelder-Maas, C., Van Thiel De Vries, J.S.M., De Vries, S., Henriquez, M., Marx, S., Ranasinghe, R., Boskalis, R., Nv, W., Water, R., En, V., Zuiderwagenplein, L., 2013. A new alternative to saving our beaches from sea-level rise: the sand engine. J. Coast. Res. 1001–1008. http://dx.doi.org/10.2112/JCOASTRES-D-13-00070.1.

Stolk, A.P., 2001. Landelijk Meetnet Regenwatersamenstelling, Meetresultaten 2000 (In Dutch). RIVM, Bilthoven, The Netherlands. Report 723101057.

Stuyfzand, P.J., 1986. A new hydrochemical classification of watertypes: principles and application to the coastal dunes aquifer system of the Netherlands., in: Proceedings of the Nineth Salt Water Intrusion Meeting. Delft, the Netherlands, pp. 641–655.

Stuyfzand, P.J., 1993. Hydrochemistry and Hydrology of the Coastal Dune Area of the Western Netherlands. Ph.D Thesis. VU Univ. Amsterdam, published by KIWA. ISBN 90-74741-01-0. http://dare.ubvu.vu.nl/handle/1871/12716, 366 pp.

Stuyfzand, P.J., Schaars, F., Van der Made, K.J., 2012a. Multitracing the origin of brackish and saline groundwaters near a dune catchment area with beach and dune nourishment (Monster, Netherlands). In: Cardoso da Silva, G., Gico de Lima Montenegro, S.M. (Eds.), 'SWIM-22-22nd Salt Water Intrusion Meeting', Proc. SWIM 22. Meta Marketing e Eventos Publ, Buzios Brazil, pp. 93–96.

Stuyfzand, P.J., Arens, S.M., Oost, A.P., Baggelaar, P.K., 2012b. Geochemische effecten van zandsuppleties in Nederland, langs de kust van Ameland tot Walcheren (in Dutch). Bosschap, The Hague, The Netherlands. Report 2012/OBN167-DK.

Templ, M., Filzmoser, P., Reimann, C., 2008. Cluster analysis applied to regional geochemical data: problems and possibilities. Appl. Geochem. 23, 2198–2213. http://dx.doi.org/10.1016/j.apgeochem.2008.03.004.

Terry, B., 1983. The acid decomposition of silicate minerals part I. Reactivities and modes of dissolution of silicates. Hydrometallurg 10 (2), 135–150.

Van Straaten, L.M.J.U., 1965. Coastal barrier deposits in south-and north-holland in particular in the areas around scheveningen and IJmuiden. Meded. Geol. Sticht. Nieuwe Ser. 17, 41–75.

Wijnakker, A.W.P., 2015. The Carbon Sequestration Capacity of the Sand Motor. Master thesis. Utrecht University, The Netherlands.